Journal of Building Engineering 114 (2025) 114288

Contents lists available at ScienceDirect

Journal of Building Engineering

journal homepage: www.elsevier.com/locate/jobe

Seismic performance of concentrically braced frames with a new Double-Stiffened-Slit Damper: a numerical investigation

Samaneh Jalal [a], Yashar Bakhshayesh [a], Bahram Mirzaie Abar [b], Reyes Garcia [c,*], Iman Hajirasouliha [d]

[a] Dept. of Civil Engineering, Science and Research Branch, Islamic Azad University, Tehran, Iran
[b] Dept. of Structures for Engineering and Architecture, University of Naples "Federico II", Naples, Italy
[c] Built Environment & Sustainability Research Cluster, School of Engineering, University of Warwick, Coventry, UK
[d] School of Mechanical, Aerospace and Civil Engineering, University of Sheffield, Sheffield, UK

ARTICLE INFO

Keywords:
Slit dampers
Concentrically braced frames (CBFs)
Energy dissipation device
Seismic behavior
Steel buildings

ABSTRACT

Strong earthquakes often produce buckling of the diagonal members of Concentrically Braced Frames (CBFs), thus reducing their energy dissipation capacity and effectiveness. This article numerically investigates the behavior of a new Double Stiffened Slit Damper (DSSD) that prevents such buckling. A new design procedure for the DSSD is first proposed. Three reference specimens (two slit dampers, one brace member) tested previously are then modeled and calibrated in Abaqus®. After calibration, the models are modified to undertake a parametric study aimed at optimizing the DSSD's strength and energy dissipation by considering different lengths, thicknesses and heights of the damper components. Subsequently, the hysteretic behavior, strength degradation, energy dissipation and plastic damage of braces with the new DSSD are investigated in Abaqus®. The numerical results indicate that braces with DSSDs have stable hysteretic behavior, without strength degradation nor buckling. The proposed DSSD also enhances the energy dissipation of the braces by up to 189% over conventional bare braces. Next, 4-, 8- and 20-story Special Concentric Braced Frames (SCBFs) with and without the new DSSDs are subjected to time-history analyses in SAP2000® using seismic records. Compared to bare SCBFs models, the SCBFs with DSSDs satisfied a Life Safety (LS) performance level and experienced (on average) up to 57.8% lower base shears. Moreover, the new DSSD effectively prevent damage to the braces by acting as a "fuse" during strong earthquakes. This article contributes towards the development of new dampers for improving the performance of steel braced buildings located in seismic areas.

1. Introduction

Many steel buildings have experienced excessive structural damage in past earthquakes [1–4]. As a result, Concentrically Braced Frames (CBFs) were introduced as a solution to reduce this damage. Despite the advantages of CBFs (e.g. good control of story drifts, and high lateral strength and stiffness), they can suffer from low energy dissipation capacity [5–8] due to the premature buckling of the diagonal braces [9–11]. This, in turn, limits the ductility of CBFs when compared to moment resisting frames [12]. To bypass these shortcomings, past research proposed the use of Buckling-Restrained Braces (BRBs) to provide more stable and symmetrical hysteretic

* Corresponding author.
E-mail address: reyes.garcia@warwick.ac.uk (R. Garcia).

https://doi.org/10.1016/j.jobe.2025.114288
Received 5 June 2025; Received in revised form 25 September 2025; Accepted 3 October 2025
Available online 9 October 2025

loops [15–17]. BRBs typically consist of a yielding core and an external restraining member, where the latter prevents buckling of the core. Generally, such restraining members are made of concrete or concrete-filled steel tubes, which often lead to heavy systems that add undesirable structural mass [18,19]. Moreover, assessing the condition of the yielding core after strong earthquakes is impossible without dismantling the BRBs themselves [20,21]. BRBs are also often built off site, which can complicate the construction process [22].

Passive control devices can reduce damage and increase the energy dissipation capacity of CBFs by up to 90% [13,14]. Among the existing passive control devices, metallic dampers are often preferred due to their cost-effectiveness, high energy dissipation capacity, and good stability to temperature changes and rate of loading. Past research has proposed numerous types of steel dampers, as shown in Figs. 1a–e. Metallic dampers are generally connected to beams using diagonal Chevron braces (Fig. 1a), including Added Damping Stiffness Dampers (ADAS) (see Fig. 1b) [23–25], ADAS with triangular plates (TADAS) (Fig. 1c) [26,27], slit dampers (Fig. 1d) [28–31], and shear dampers (Fig. 1e) [32–35]. Whilst shear dampers have higher initial stiffness and energy dissipation capacity compared to ADAS dampers, their tendency to buckle under large deformation results in an unstable hysteretic response [36]. To address this drawback, several studies have investigated the mechanical behavior of slit dampers as a potential solution to minimize buckling of shear dampers [36]. However, the combination of (lateral) seismic and vertical loads can cause large beam deflections (see Figs. 2a–b), which affect negatively the performance of the damper [37,38]. To address these problems, recent studies have proposed new alternative bracing systems. For example, Taiyari et al. [39] investigated experimentally and numerically the behavior of U-shaped dampers bolted to the full length of the brace (see Fig. 3a). The results indicate that this bracing system offers stable hysteresis response at large inelastic deformations. Similarly, Askariani and Garivani [40] investigated numerically the performance of a new brace-slit damper in which two diagonal double-channel members surround the steel slit plates (Fig. 3b). Such damping system provides full hysteresis curves and can be used as an energy dissipation device. Beheshti Aval et al. [41] proposed a novel Fan Bracing System (FBS) with several steel discs connected to a central shaft (Fig. 3c). Numerical results showed that the energy dissipation capacity of the FBS was about 15% higher than that of conventional BRB. Although these energy dissipation devices can improve the behavior of CBFs, the use of numerous metallic devices along the full length of the brace can lead to a heavy and expensive damping system [22].

More recently, Gray et al. [42] proposed a Yielding Brace System (YBS) with cast steel "fingers" placed at the ends of diagonal braces (Fig. 3d). The YBS system effectively prevents brace buckling by dissipating seismic energy through the flexural yielding of the steel "fingers". Albakkar and Behnamfar [43] introduced a new Grooved Gusset Plate Damper (GGPD) (Fig. 3e) with X-shaped braces. The hysteretic behavior of the GPPD was investigated using Abaqus® software and the results indicated that the GGPD dissipated about twice the amount of energy of a normal CBF. Likewise, Pachideh et al. [44] proposed a system consisting of a ring yielding damper and diamond-shaped braces (Fig. 3f). The proposed bracing system had around 45% higher energy dissipation capacity than the CBF. While these studies developed effective yielding systems to improve the seismic behavior of the CBFs, the special shape of the dampers can make them expensive and challenging to manufacture in practice [45]. As a result, more practical solutions are needed to improve the behavior of CBFs. Among the different dampers, Steel Slit Dampers (SSD) are deemed as a cost-effective solution as they have the advantageous features of shear dampers but without their drawbacks [36,40].

This study numerically investigates the performance of a new metallic Double Stiffened Slit Damper (DSSD). Unlike previous dampers, the new DSSD connects directly to the diagonal bracing member. As such, the performance of the DSSD is unaffected by the floor beam, which in turn improves the system's seismic performance. A new design procedure for the DSSD is first proposed. Three reference specimens (two slit dampers, and one brace member) tested previously are then modeled and calibrated in Abaqus® software. After calibration, the models are modified to undertake a parametric study aimed at optimizing the DSSD's strength and energy dissipation by considering different lengths, thicknesses and heights of the damper components. The DSSD is then fitted to bare braces

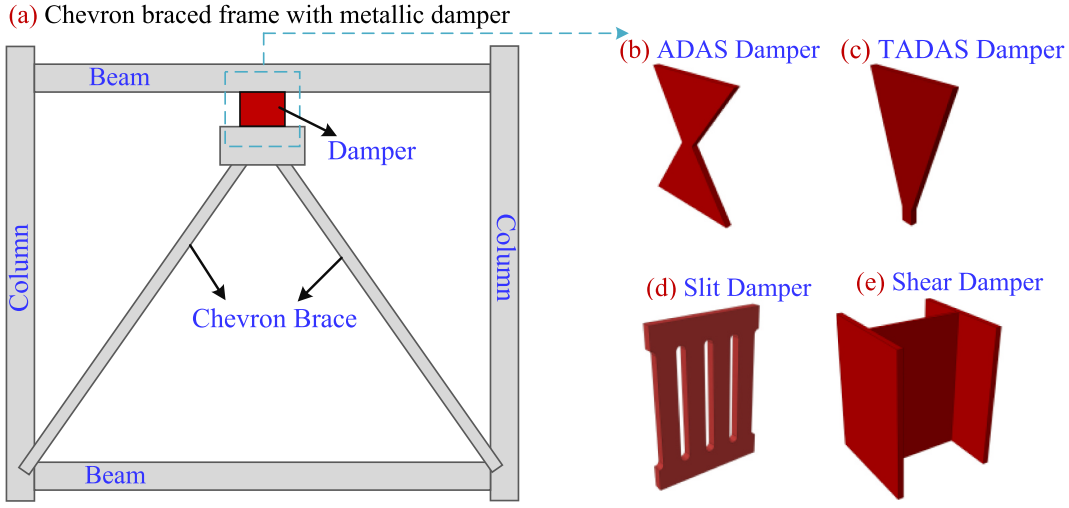

Fig. 1. (a) Typical metallic dampers in CBFs, (c)–(e) different types of common dampers.

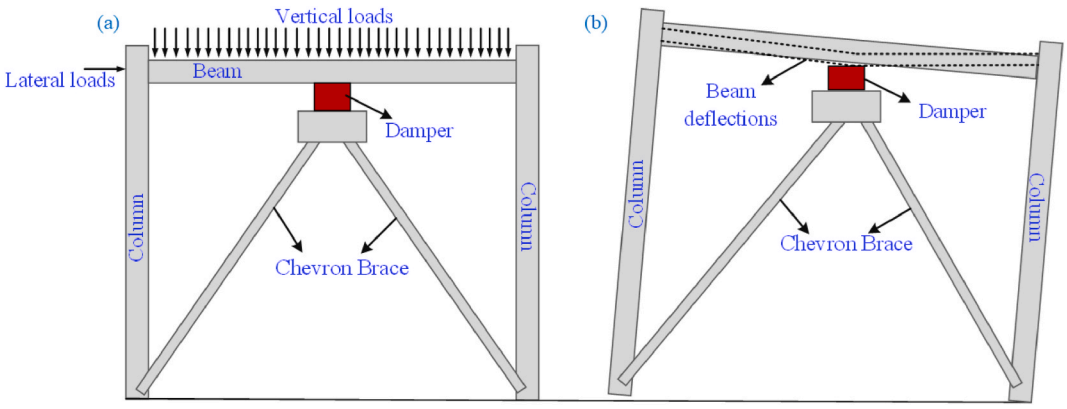

Fig. 2. (a) Combined effect of lateral and vertical loads, and (b) beam deflections due to such effects.

to investigate the improvements in their hysteretic performance in Abaqus®. Finally, nonlinear time history analyses on 4-, 8- and 20-story Special Concentrically Braced Frames (SCBFs) with and without DSSD are carried out using SAP2000® to assess the effectiveness of the damper at controlling damage and drifts.

2. A new Double Stiffened Slit Damper (DSSD)

Fig. 4 shows the main components of the DSSD, which consists of: (a) slit plates, (b) stiffeners, (c) a middle plate, (d) boundary plates, and (e) a main core. The DSSD dissipates the seismic energy through plasticity in the slit dampers and stiffeners, whereas the middle plate, boundary plates and core do not resist load. Fig. 5 shows the proposed location of the DSSD in the CBF and corresponding fabrication details. Fillet welds are proposed to assemble the components of the DSSD. Different types of sections (e.g. box, I or circular) can be used as diagonal braces due to the geometry of the damper, thus giving versatility to the system. The core of DSSD can be connected to the brace by welding and bolts. Likewise, the brace with the DSSD can be bolted to a gusset plate. Bolted connections facilitate the replacement of the damper after a strong seismic event. Unlike traditional metallic dampers which are usually placed between the Chevron braces and the floor beam, Fig. 5 shows that the DSSD is placed at the bottom end of the diagonal brace, and therefore its performance is not influenced by the frame's beam. Moreover, bolts connect the DSSD to the brace or gusset plate, leading to easier installation and replacement after an earthquake compared to other dampers (e.g. BRB). The DSSD can also be attached to the bracing member beforehand, thus eliminating the need of on-site overhead and vertical welding. As it will be shown later, the new damper effectively prevents buckling of bracing members by concentrating damage at the damper, whereas the braces remain within the elastic range.

2.1. Design method for new DSSD

Fig. 6a shows the behavior of an individual strut of width b and height h subjected to a lateral load, which replicates the proposed damper. Struts with low h/b ratios exhibit primarily shear-controlled responses, whereas higher h/b ratios activate coupled shear-bending mechanisms [46]. Consequently, each strut sustains specific shear forces and bending moments under cyclic loading. The corresponding deformation (δ) can be derived according to Eq. (1) (see Fig. 6a):

$$\delta = \frac{Ph^3}{12EI} + \frac{Ph}{5/6 \times b \times t \times G} \tag{1}$$

where E is the elastic modulus (taken as approximately 2.5 times of shear modulus G); t, b and h are the thickness, width and height of the strut, respectively; and I is the moment inertia of the strut. By rearranging parameters, the deformation (δ) and stiffness of the slit dampers (K_{slit}) can be determined as [28,46,47]:

$$\delta = \frac{Ph^3}{Etb^3} \times \left(1 + 3\frac{b^2}{h^2}\right) \tag{2}$$

$$K_{slit} = \frac{nEtb^3}{h^3\left(1 + 3\frac{b^2}{h^2}\right)} \tag{3}$$

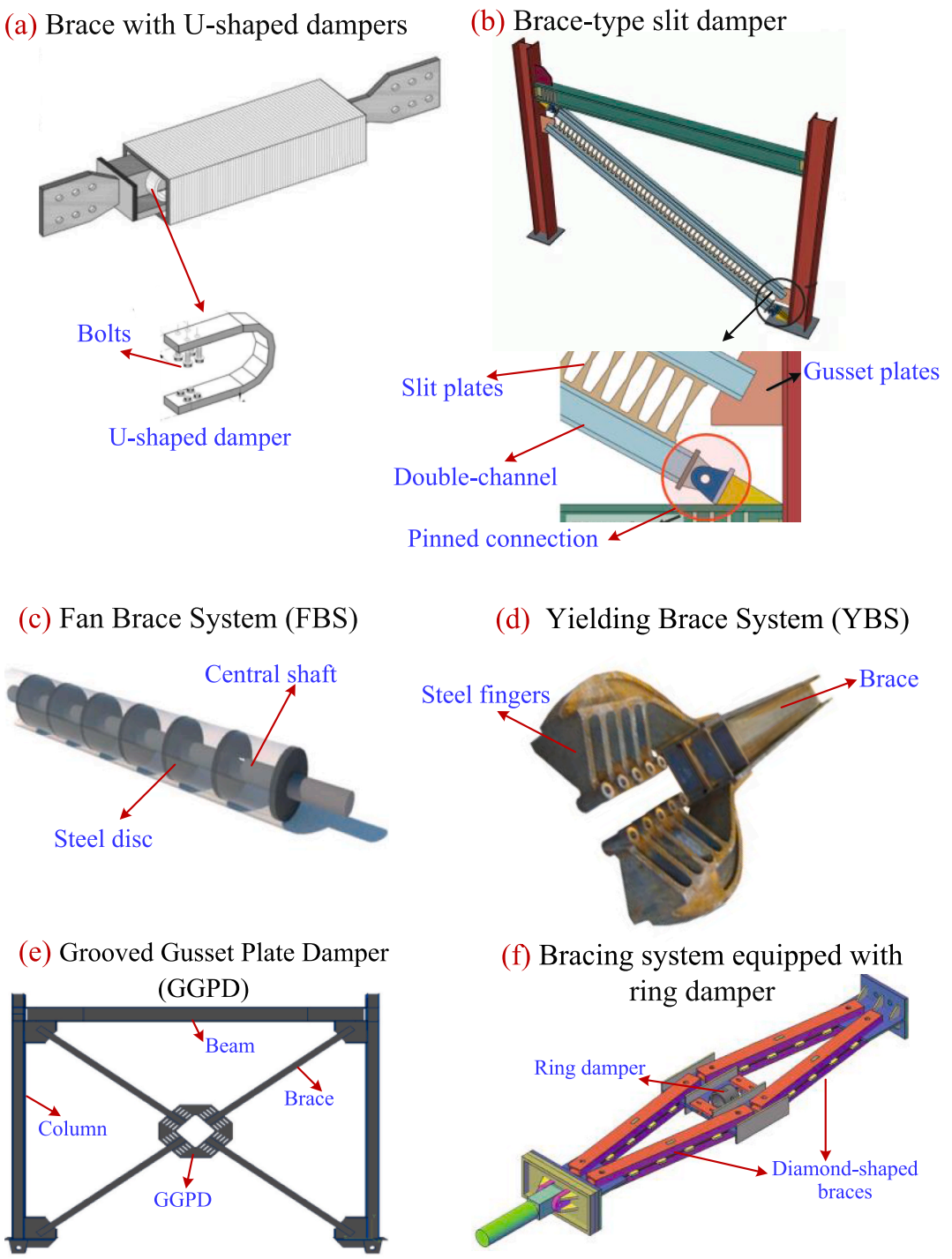

Fig. 3. (a) Brace with U-shape dampers [39], (b) brace-type slit damper [40], (c) Fan Brace System (FBS) [41], (d) Yielding Brace System (YBS) [42], (e) Grooved Gusset Plate Damper (GGPD) [43], bracing system with ring damper [44].

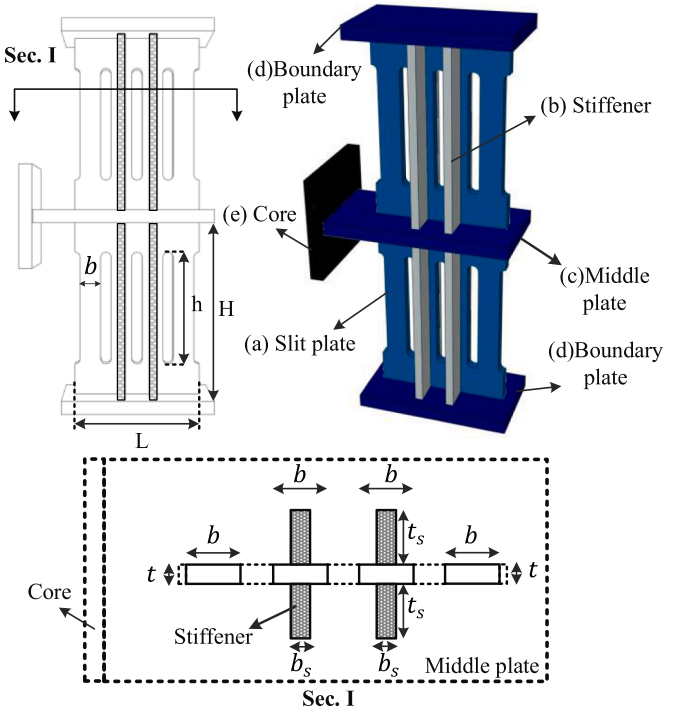

Fig. 4. Schematic side and 3D view of new DSSD.

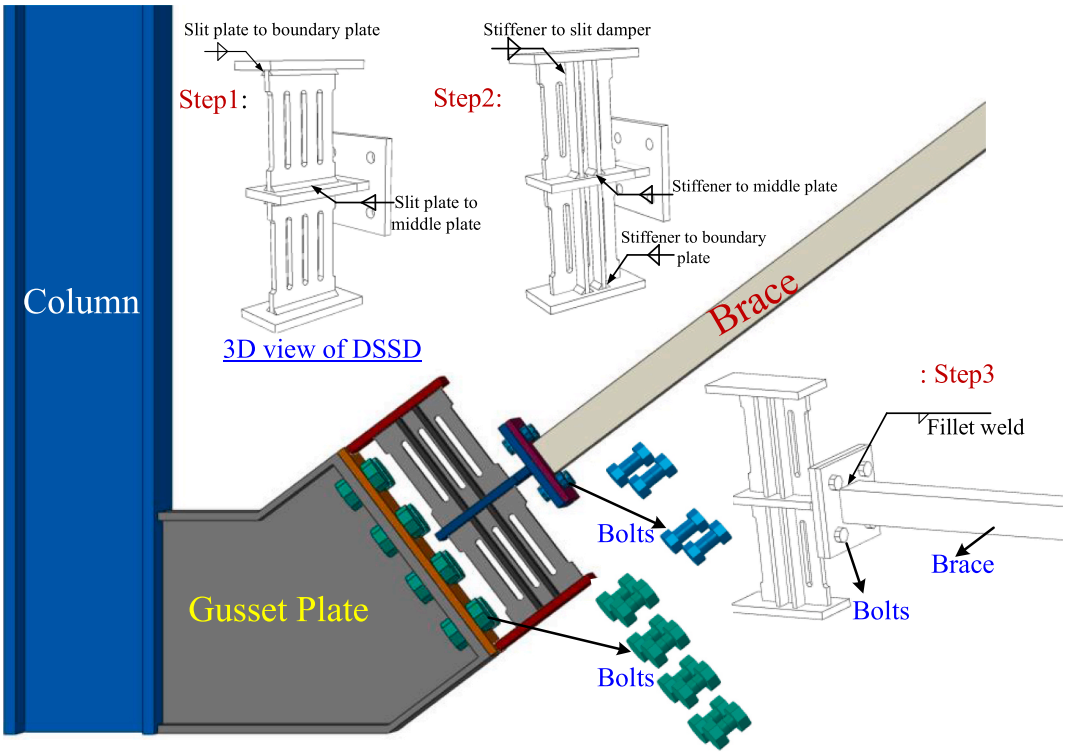

Fig. 5. Location of DSSD in the CBF and fabrication details.

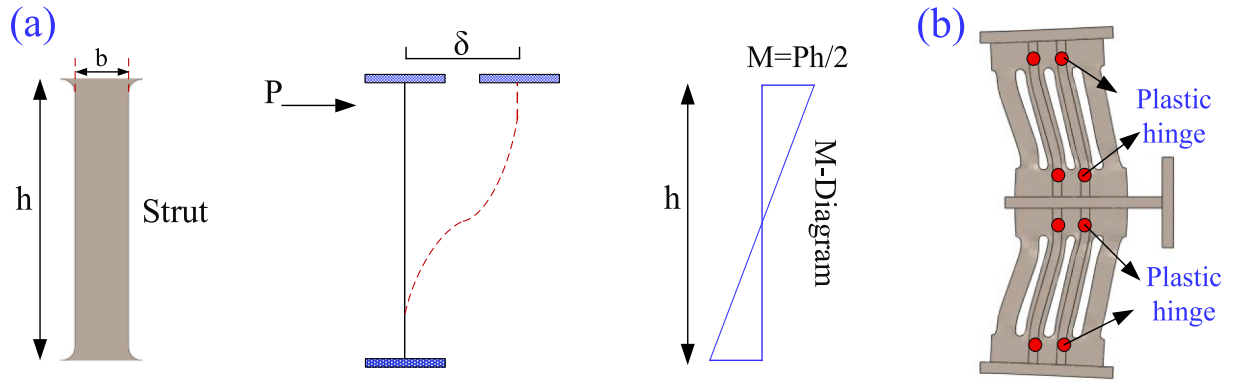

Fig. 6. Mechanism of DSSD under lateral load: (a) strut, (b) stiffener.

where n is the number of struts. Flexural plastic hinges are expected to develop at both ends of the stiffeners (see Fig. 6b). Based on this assumption and on classical structural analysis theory, the stiffness of the stiffener (K_{stiff}) and total stiffness of the DSSD (K_{DSSD}) are calculated as [48]:

$$K_{stiff} = \frac{n' 12EI}{H^3} \tag{4}$$

$$K_{DSSD} = K_{slit} + K_{stiff} \tag{5}$$

where n' is the number of stiffeners; whereas I and H are the moment inertia and height of the stiffener, respectively.

The design method assumes that, under seismic loads, the DSSD experiences inelastic deformations, whereas the bracing member

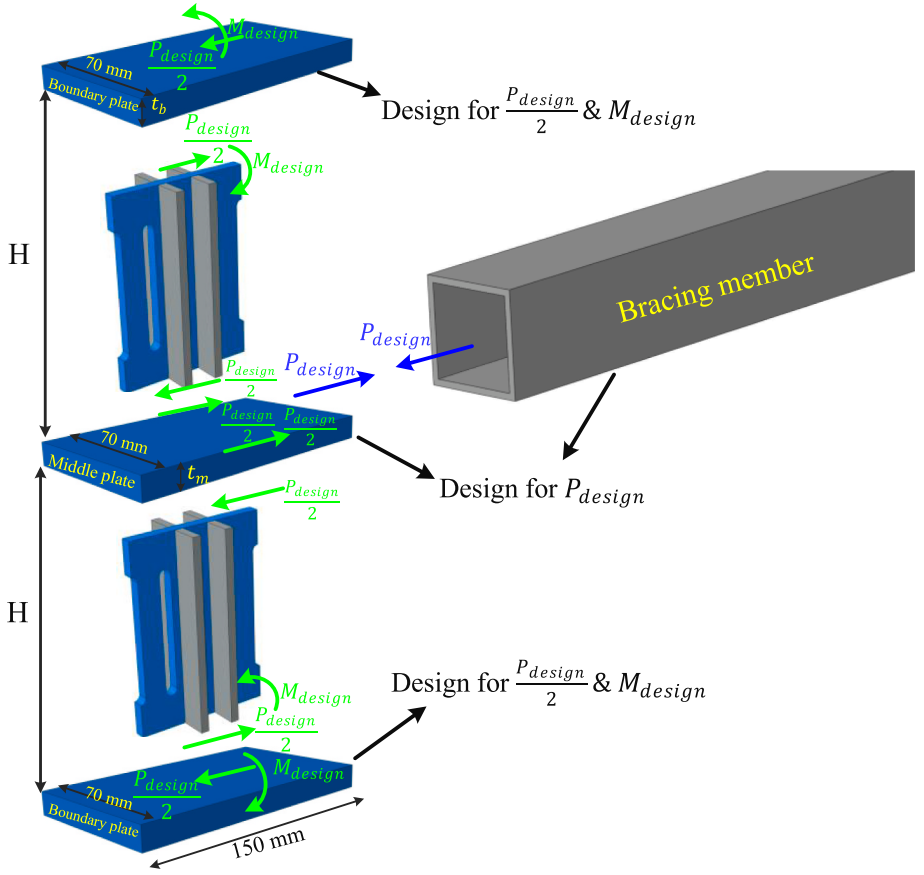

Fig. 7. Free body diagram to design DSSD.

remains elastic. As such, large inelastic deformations (plastic behavior) are expected to occur in the slit plates and stiffeners, but without strength degradation. By ignoring strain hardening effects, the yield strength of the DSSD (P_y) can be calculated as [29]:

$$P_{y1} = min\left\{\frac{nF_y tb^2}{2h}, \frac{2nF_y tb}{3\sqrt{3}}\right\} \tag{6}$$

$$P_{y2} = min\left\{\frac{n'F_y t_s b_s{}^2}{2H}, \frac{2n'F_y t_s b_s}{3\sqrt{3}}\right\} \tag{7}$$

$$P_y = P_{y1} + P_{y2} \tag{8}$$

where P_{y1} and P_{y2} are the yield strengths for slit dampers and stiffeners, respectively; n and n' are the number of struts and stiffeners, respectively; F_y is the yield stress of steel; h and H, respectively, are the height of the struts and stiffeners (see Fig. 4); t and t_s are the thickness of the slit dampers and stiffeners, respectively; and b and b_s are the struts width and stiffeners width, respectively (Fig. 4).

To ensure that the DSSD works as a ductile "fuse" in a frame, the elements outside the damper should be designed according to the maximum strength of the damper (P_{design}), as specified in Eq. (9):

$$P_{design} = \Omega_0 P_y \tag{9}$$

where Ω_0 is an overstrength factor, as defined in the next sections.

The yielding of the DSSD should govern the behavior of the system. Therefore, the bracing member is designed to resist a force higher than the capacity of the damper according to the following equation:

$$P_{design} \leq \Phi P_n \tag{10}$$

where Φ is a reduction coefficient for compressive strength ($\Phi = 0.9$ in AISC 360-16 [49]); and P_n is the nominal compressive strength of the bracing member according to AISC 360-16. The value P_n can be calculated using Eq. (11a) or Eq. (11b):

$$P_n = \left(0.658^{\frac{F_y}{F_e}}\right) F_y A_g \;\; ; \;\; \text{if} : \frac{F_y}{F_e} \leq 2.25 \tag{11a}$$

$$P_n = 0.877 F_e A_g \;\; ; \;\; \text{if} : \frac{F_y}{F_e} > 2.25 \tag{11b}$$

where A_g is the gross cross-sectional area of the bracing member; and F_e is the elastic buckling stress of the brace, which can be calculated using Eq. (12).

$$F_e = \frac{\pi^2 E}{\left(\frac{L_c}{r}\right)^2} \tag{12}$$

where E is the modulus of elasticity of steel; L_c is the effective length of the brace; and r is the radius of gyration of the bracing member section.

Fig. 7 shows the free body diagram with the forces of the DSSD. Fig. 7 shows that the middle plate is subjected to P_{design} (axial force), which can be designed similarly to the bracing member according to Eq. (10). The boundary plates are subjected to $\frac{P_{design}}{2}$ (axial force) and M_{design} (bending moment). The value of P_{design} can be derived from Eq. (9), whereas M_{design} can be determined using the relationship

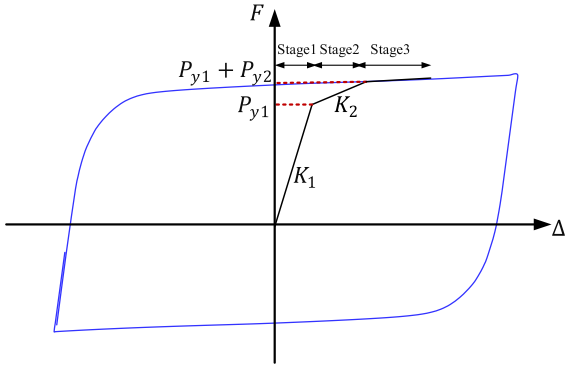

Fig. 8. Idealized hysteretic response of the DSSD.

$M_{design} = \frac{P_{design}}{2} \times H$. The boundary plates should be designed to withstand a combination of axial force and bending moment. Therefore, the following equations should be used in accordance with AISC 360-16 [49]:

$$\frac{P_r}{P_c} + \frac{8}{9}\frac{M_r}{M_c} \leq 1 \quad \text{if} : \frac{P_r}{P_c} \geq 0.2 \tag{13a}$$

$$\frac{P_r}{2P_c} + \frac{M_r}{M_c} \leq 1 \quad \text{if} : \frac{P_r}{P_c} < 0.2 \tag{13b}$$

where P_r and M_r are the $\frac{P_{design}}{2}$ and M_{design} , respectively; and P_c and M_c are the compression and bending strength of the boundary plates, respectively. It should be noted that the boundary plates and middle plate are assumed to have similar width and length. The thickness of the boundary plate (t_b) and middle plate thickness (t_m) are obtained by applying the previous equations. For illustrative purposes, Appendix A presents a design example of a DSSD.

Fig. 8 shows the idealized hysteretic response of the DSSD. Since the slit dampers and stiffeners may have different yield levels, this response can be defined by a trilinear model. Initially, both slit dampers and stiffeners behave elastically. Hence, the stiffness of the DSSD in this stage (K_1) is characterized by K_{DSSD} (Eq. (5)). Once the force reaches P_{y1}, the slit dampers yield, whereas the stiffeners remain elastic. The stiffness at this stage (K_2) is the sum of post yield stiffness of the slit dampers and the elastic stiffness of the stiffeners (K_{stiff}). Finally, after the force increases to $P_{y1} + P_{y2}$, both slit dampers and stiffeners enter the plastic stage, thus providing energy dissipation capability.

3. Finite element analyses

Nonlinear numerical analyses are carried out using Abaqus® software [50] considering two Stages.

1) Stage 1: Two steel slit dampers (DSSH2 and DSSH3) tested previously by Nik-Hoosh and Kafi [30,31], and a steel brace member (40×40×3×1250 CS-HR) tested by Nipe et al. [51] were modeled. These models serve as a benchmark that replicate the hysteric behavior and damage of slit dampers and bracings.
2) Stage 2: A set of DSSDs were designed to conduct a parametric study. Subsequently, DSSDs were then attached to a brace member to assess its seismic behavior.

3.1. Modeling approach

8-node linear cubic elements (C3D8R) with reduced integration were adopted for the mesh [50]. To determine an optimal mesh, the mesh size was evaluated through mesh sensitivity analyses, as shown in Fig. 9. In this figure, the error represents the difference in maximum strength between the experimental and FE results. Based on this analysis, mesh sizes of 5 mm and 7 mm were selected for the slit dampers [30,31] and the brace [51], respectively. This resulted in 2542 elements (4419 nodes) for the slit damper model [30,31] and 11,368 elements (17,496 nodes) for the brace model [51]. Fig. 10 shows the boundary conditions and loading protocol used in the

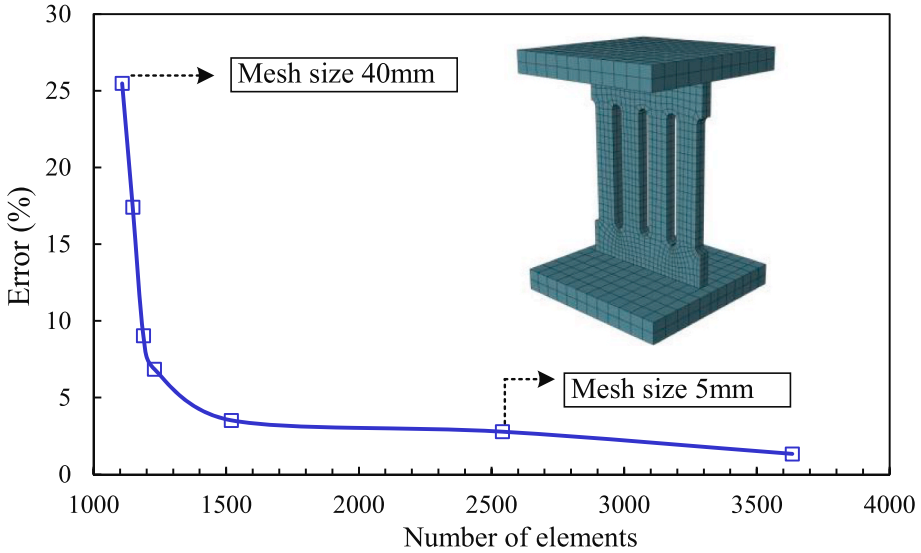

Fig. 9. Mesh sensitivity analyses.

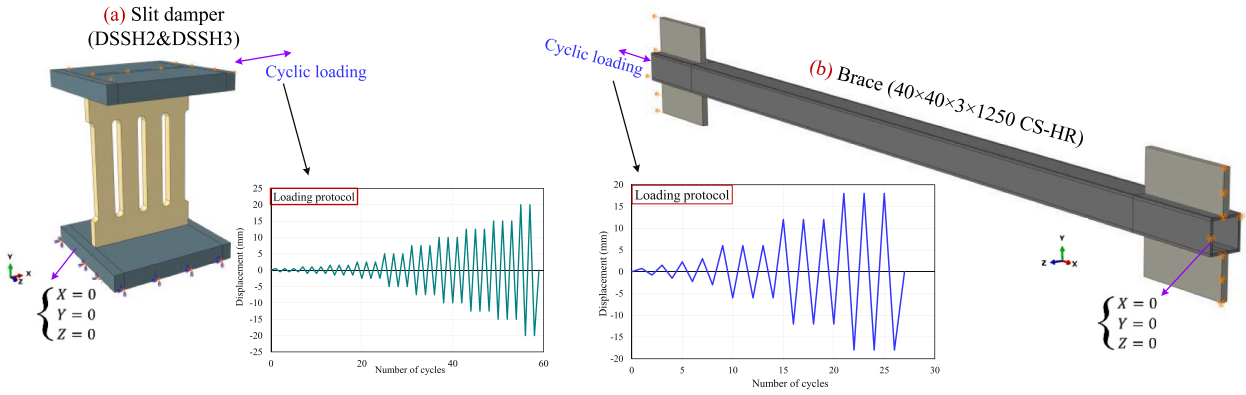

Fig. 10. Boundary conditions and loading protocol of modeled specimens: (a) slit dampers DSSH2 & DSSH3 (adapted from Refs. [30,31]), (b) brace 40×40×3×1250 CS-HR (adapted from Ref. [51]).

Table 1
Steel properties used in Abaqus® modeling.

Specimen	Young's modulus E (GPa)	Poisson's ratio υ (−)	Yield stress F_y (MPa)	Ultimate stress F_u (MPa)
Slit damper [30,31]	200	0.3	250	470
Brace [51]	200	0.3	360	520

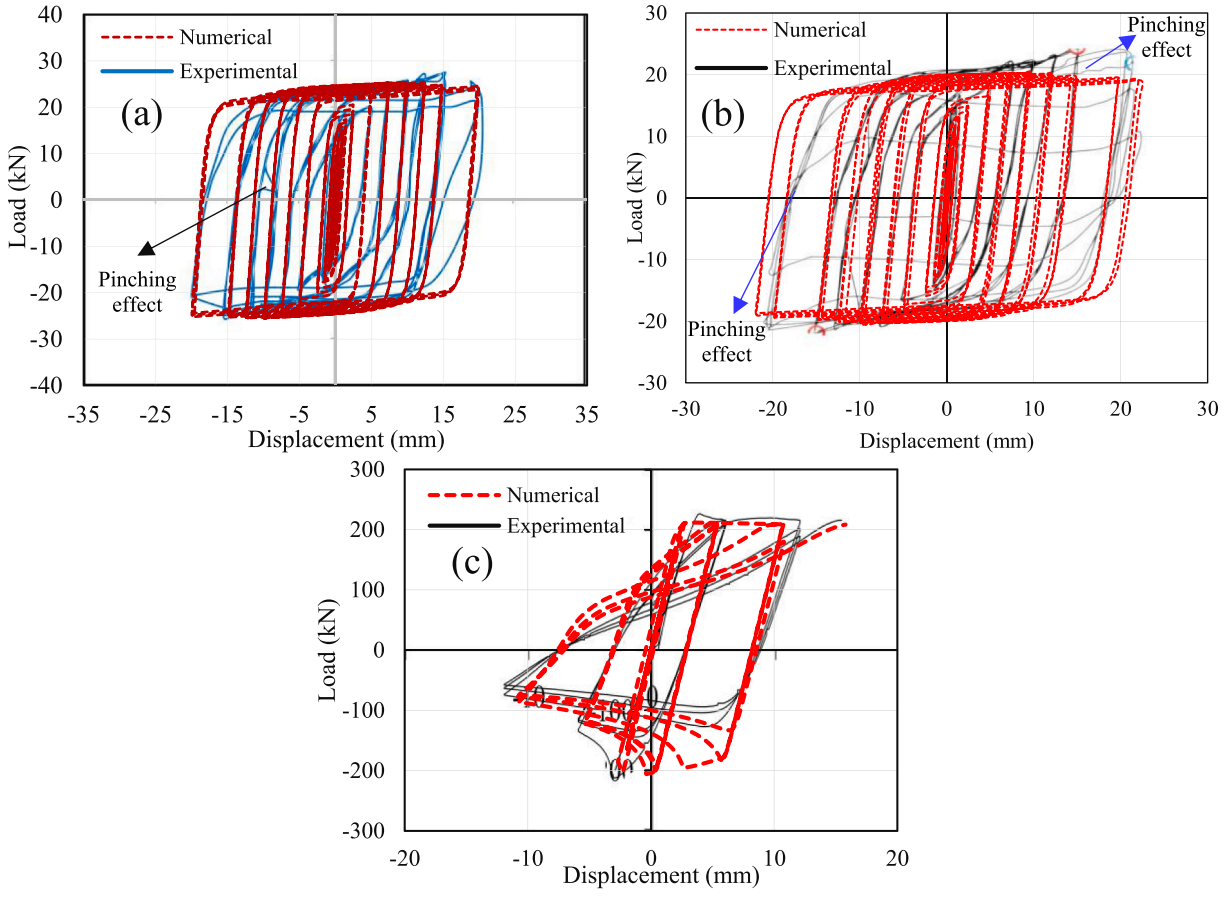

Fig. 11. Numerical vs experimental load-displacement curves of specimens: (a) DSSH2 [30,31], (b) DSSH3 [30,31], and (c) 40×40×3×1250 CS-HR [51].

analysis [30,31,51]. A general static analysis based on the full Newton-Raphson method was adopted [50]. The steel material was modeled using a bilinear stress-strain curve with isotropic-hardening plastic behavior [50]. Table 1 summarizes the Poisson's ratio, Young's moduli, yield stress and ultimate stress of the steel material used in the analysis. A plasticity model with a von Mises yielding surface was used [50]. To allow for buckling in the brace models, initial imperfections were also considered [50]. The amplitude of imperfections was considered as $L_B/1000$, where L_B is the length of the brace, as suggested in past research [52]. To achieve this, an elastic buckling analysis was first performed, and then the first eigenmode of each model was applied. It should be mentioned that the numerical models developed in this study assume perfect bolted connections using tie constraints. This was done because only axial force is assumed to be transmitted between the brace and damper (and also between the damper and end plate). However, connections where shear force is transmitted between the connection's components can introduce some slippage and flexibility to the damper. This, in turn, is expected to reduce the stiffness of the damper, as well as to degrade its hysteretic response more rapidly.

3.2. Stage 1: calibration of numerical models with experimental results

Figs. 11a–c compare the load-deflection results from Abaqus® and the experimental results of specimens DSSH2 (Fig. 11a), DSSH3 (Figs. 11b) and 40×40×3×1250 CS-HR (Fig. 11c). The results in Figs. 11a–b indicate that the numerical models of the slit dampers match very well the experimental hysteresis curves. However, some minor differences are observed due to "spiking" effects, which are difficult to capture in the model. Indeed, past studies (e.g. [72,73]) have demonstrated that these effects result from a slight tilt in the loading device, or from slippage in the steel plates of the specimen, leading to local crimping in the hysteresis curve. Fig. 11c shows that Abaqus® can also simulate well the strength reduction due to buckling of the brace element. It should be noted that out-of-plane deformation was not considered in the modeling since this was negligible in the reference specimens used in this study. However, such effect can have a significant impact on the hysteretic response of slit dampers, and therefore it should be considered for other cases different to those analyzed here.

In this study, an equivalent plastic strain (PEEQ) approach was adopted to assess failure modes in the Abaqus® models [50]. Past research suggested that PEEQ is suitable to assess damage of experimental specimens [4,10,53,54]. Figs. 12a–c compare the PEEQ distribution from Abaqus® and the corresponding experimental results of specimens DSSH2 (Fig. 12a), DSSH3 (Figs. 12b) and 40×40×3×1250 CS-HR (Fig. 12c). As shown in Figs. 12a–b, the maximum PEEQ value for DSSH2 and DSSH3 specimens are 11.38 and 9.13, respectively, as highlighted in green. The lower PEEQ value (PEEQ = 9.13) is selected as a benchmark to evaluate the damage situation in the numerical models of the DSSD [4,10,53,54], as discussed later. The results in Figs. 12a–b show that most of the plastic demand in the slit dampers occurs at the corner of the struts, which matches well the damage observed in the experiments. This confirms that the finite element models in Abaqus® capture well the damage experienced in slit dampers. Likewise, the results in Fig. 12c indicate that the numerical model simulated well the buckling deformation experienced by the brace during the experiments.

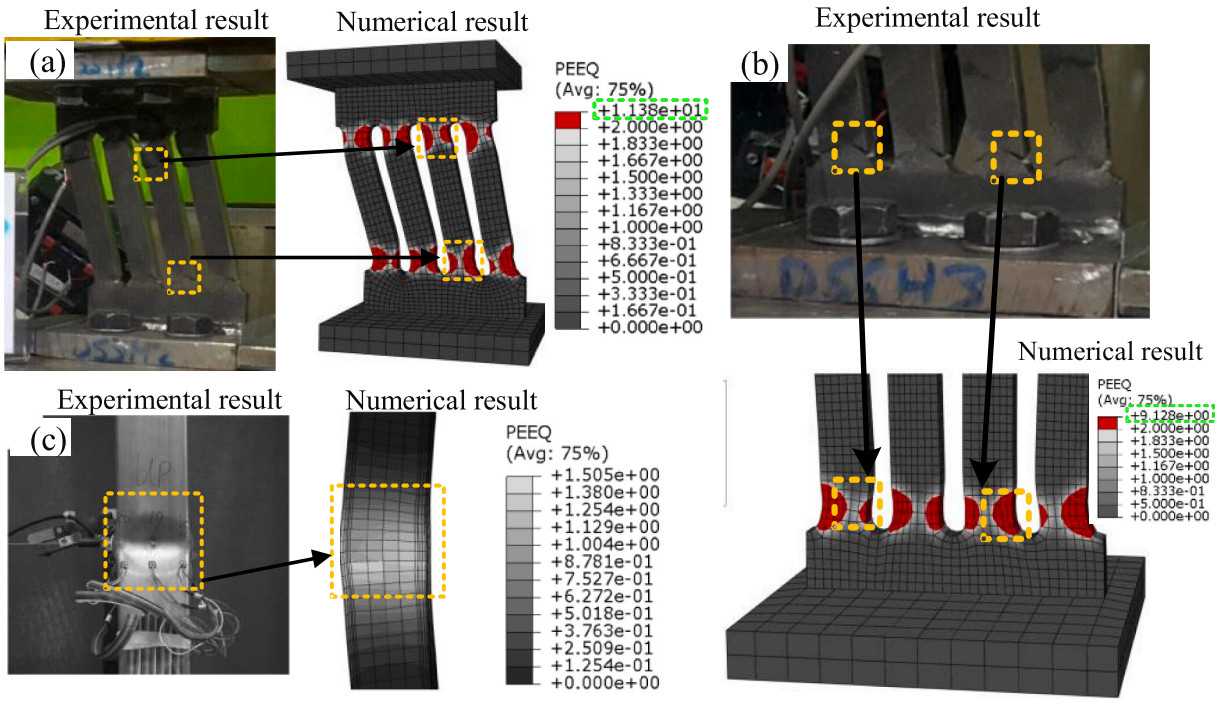

Fig. 12. Numerical PEEQ distribution vs experimental damage of specimens: (a) DSSH2 [30,31], (b) DSSH3 [30,31], and (c) 40×40×3×1250 CS-HR [51].

It can be concluded that the Abaqus® models simulate well the overall hysteretic behavior and local failure modes of slit dampers and brace elements. Consequently, such models can be further extended to investigate the behavior of the new DSSD fitted on braces.

3.3. Stage 2: modeling of DSSD

A similar modeling approach as that described in section 3.2 was adopted to model the DSSD in Abaqus®. However, the boundary conditions, meshing and loading protocol were modified accordingly. The boundary conditions were determined based on the real conditions of the DSSD in a steel frame (see Fig. 13a). Therefore, the end of the boundary plates (which are attached to the gusset plate) were restricted against rotation and displacement (i.e. a fixed support was considered). Fig. 13b shows the meshing of the DSSD model. The DSSD models had a 5 mm mesh size, leading to 8500 elements and 12,000 nodes on average. This mesh size was sufficient to simulate the experimental results of the slit dampers, as shown in Stage 1. Cyclic "loading" was applied at the end of the middle plate of the DSSD, where the damper is connected to the brace member. Fig. 14 shows the displacement control protocol applied to the Abaqus® models, in accordance with FEMA-461 [55]. The amplitude of each cycle increased by 40% compared to the previous cycle [55], thus leading to the following displacements: 0.96, 1.35, 1.89, 2.65, 3.71, 5.19, 7.27, 10.0, 14.0 and 20.0 mm. The maximum displacement of the cyclic loading protocol was considered as $\Delta m = 20$ mm, based on the test results by Nik-Hoosh and Kafi [30,31].

3.4. Parametric models

A parametric analysis was undertaken to optimize the DSSD's performance and maximize their strength and energy dissipation. Table 2 summarizes the details and properties of the nineteen models chosen for the analysis. Note that the dimensions of the slit plates of model DSSDM were selected based on specimen DSSH2 tested by Nik-Hoosh and Kafi [30,31]. Hence, in Table 2, model DSSDM serves as a benchmark for the new DSSD proposed in this study. Other models in Table 2 were created by changing the length, thickness and height of the damper, as well as the struts' width (see Fig. 4), all of which were expected to change the damper's behavior.

4. Numerical results of parametric analysis and discussion

4.1. Hysteretic behavior and energy dissipation

Figs. 15a-r, Figs. 16a–f and Figs. 17a–f compare, respectively, the hysteretic curves (force-displacement), energy dissipation and stiffness of the DSSD models in Abaqus®. The last four columns of Table 2 also summarize the maximum strength, energy dissipation, over strength factor (Ω_0) and stiffness of such models. The hysteresis curves in Figs. 15a–c show that, by increasing the thickness of the slit plates (t) from 8 mm (model DSSDM) to 12, 16, and 20 mm, the maximum strength increases by 40.9% (model DSSDt12), 83.6% (DSSDt16), and 126.2% (DSSDt20), respectively. Likewise, a 2.5 times increase of t from 8 mm to 20 mm enhances the energy dissipation and stiffness by 133% and 230%, respectively (see Figs. 16a and 17a). The results in Figs. 15d–f show that an increase in the slit plates' length L from 100 mm (DSSDM) to 150, 200 and 250 mm results in a 72.8% (DSSDL150), 138.9% (DSSDL200), and 207.3% (DSSDL250) improvement in strength, respectively. Moreover, increasing L from 100 mm to 250 mm (2.5 times) enhances the energy

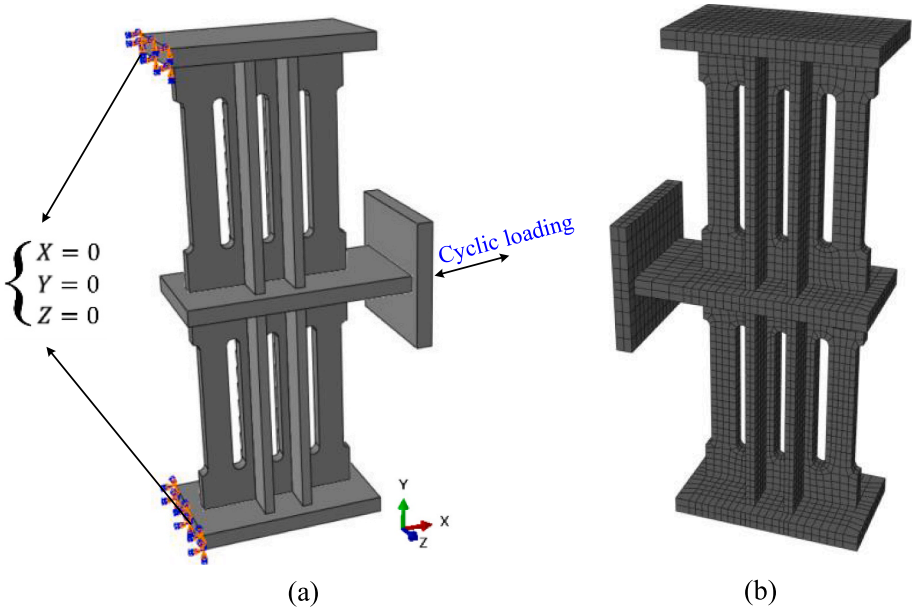

Fig. 13. Details of DSSD in Abaqus®: (a) boundary conditions, and (b) meshed components.

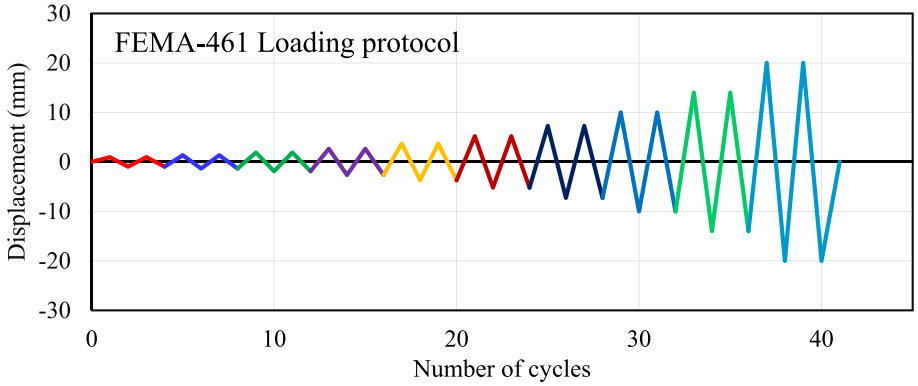

Fig. 14. Loading protocol applied in numerical analyses of DSSD [55].

Table 2
Details of DSSD models in Abaqus®.

Model ID	Damper dimensions (mm)									Cyclic results			
	L	t	H	h	b	b_s	t_s	n	n'	Maximum strength (kN)	Energy dissipation (kN.m)	Overstrength factor (Ω_0)	Stiffness (kN/mm)
DSSDM[a]	100	8	140	90	16.5	6	20	8	8	62.53	23.67	2.13	27.65
DSSDt12	100	12	140	90	16.5	6	20	8	8	88.13	33.86	2.12	60.52
DSSDt16	100	16	140	90	16.5	6	20	8	8	114.81	44.74	2.14	82.26
DSSDt20	100	20	140	90	16.5	6	20	8	8	141.45	55.25	2.15	91.29
DSSDL150	150	8	140	90	16.5	6	20	12	16	108.03	40.78	2.31	53.23
DSSDL200	200	8	140	90	16.5	6	20	16	24	149.38	55.84	2.33	70.17
DSSDL250	250	8	140	90	16.5	6	20	20	32	192.13	65.63	2.36	102.78
DSSDH90	100	8	90	58	16.5	6	20	8	8	109.42	43.69	2.36	81.65
DSSDH190	100	8	190	122	16.5	6	20	8	8	42.80	14.63	1.98	20.22
DSSDH240	100	8	240	154	16.5	6	20	8	8	31.71	9.51	1.86	9.10
DSSDb11.5	100	8	140	90	11.5	6	20	10	12	55.24	19.11	2.07	21.76
DSSDb8	100	8	140	90	8.0	6	20	12	16	52.53	16.96	2.14	17.04
DSSDb6	100	8	140	90	6.0	6	20	14	20	52.12	16.38	2.04	15.27
DSSDbs8	100	8	140	90	16.5	8	20	8	8	74.42	27.07	1.94	34.94
DSSDbs10	100	8	140	90	16.5	10	20	8	8	86.59	31.32	1.87	40.20
DSSDbs12	100	8	140	90	16.5	12	20	8	8	102.65	36.92	1.83	43.88
DSSDts23	100	8	140	90	16.5	6	23	8	8	67.96	24.96	2.03	30.84
DSSDts26	100	8	140	90	16.5	6	26	8	8	68.65	25.17	1.98	31.02
DSSDts29	100	8	140	90	16.5	6	29	8	8	71.86	26.05	2.00	31.10

[a] Benchmark model of DSSD.

dissipation and stiffness by 177% and 272%, respectively (see Figs. 16b and 17b). The results in Figs. 15g–i also show that as the height of the damper h increases, the hysteretic response, strength, energy dissipation and stiffness of the DSSD decrease. For instance, increasing h from 90 mm (DSSDM) to 240 mm (DSSDH240) reduces the damper strength by up to 71% (see Fig. 15i), the energy dissipation by 78% (Fig. 16c) and the stiffness by 89% (Fig. 17c). The results in Figs. 15j-l shows that reducing the width of the struts b has a minor influence on the hysteresis response. Nevertheless, reducing b from 16.5 mm (DSSDM) to 6 mm (DSSDb6) leads to a 16.6% (Fig. 15l), 31% (Fig. 16d) and 44% (Fig. 17d) decrease in strength, energy dissipation and stiffness, respectively. Figs. 15m-o compare the effect of stiffener thickness b_s on the cyclic response of the DSSD. It is shown that an increase in b_s from 6 mm to 12 mm improves the damper strength by up to 64.2% (DSSDM vs DSSDbs12 in Fig. 15o), the energy dissipation by 56% (Fig. 16e) and stiffness by 59% (Fig. 17e). The hysteresis curves in Figs. 15p-r show that increasing t_s from 20 mm to 29 mm does not significantly affect the hysteresis loops. However, the strength, energy dissipation and stiffness of DSSDts29 increase marginally by 15%, 10% and 12%, respectively, compared to DSSDM.

Based on the above results, it can be concluded that the new DSSD proposed in this study has robust and stable hysteresis loops, thus being suitable to dissipate energy. Overall, the results in Figs. 15a-r shows that the stiffness and strength only degrade during the last cycles of the response. The results from the parametric analysis also indicate that, to maximize the strength and energy dissipation capacity of the DSSD, the parameter h should be kept small, whereas t and L should be large.

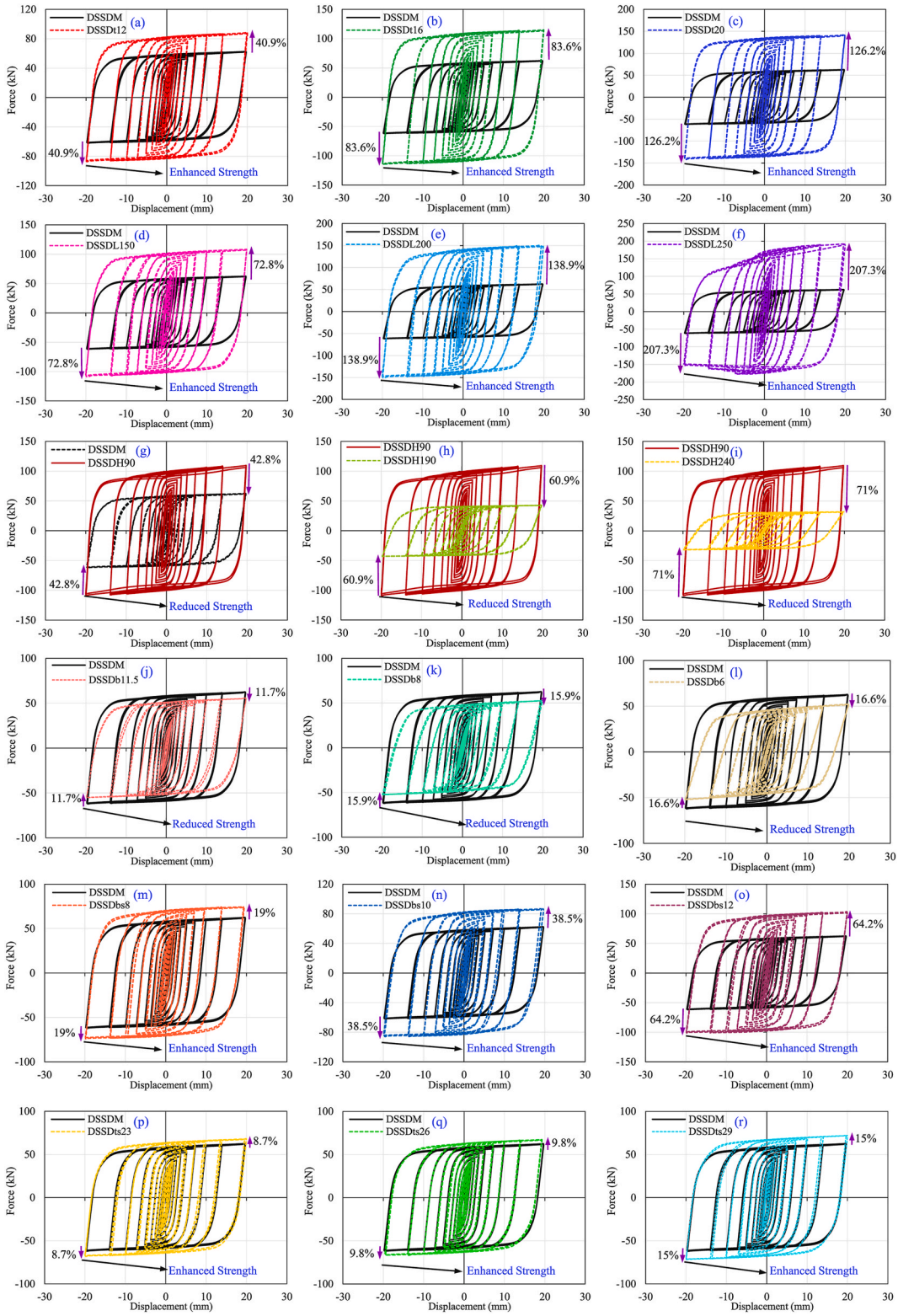

Fig. 15. Force-displacement hysteresis loops of DSSD with different: (a)–(c) thickness of slit plates t, (d)–(f) slit plates length L, (g)–(i) height of struts h, (j)–(l) struts width b, (m)–(o) stiffeners width b_s, and (p)–(r) stiffeners thickness t_s.

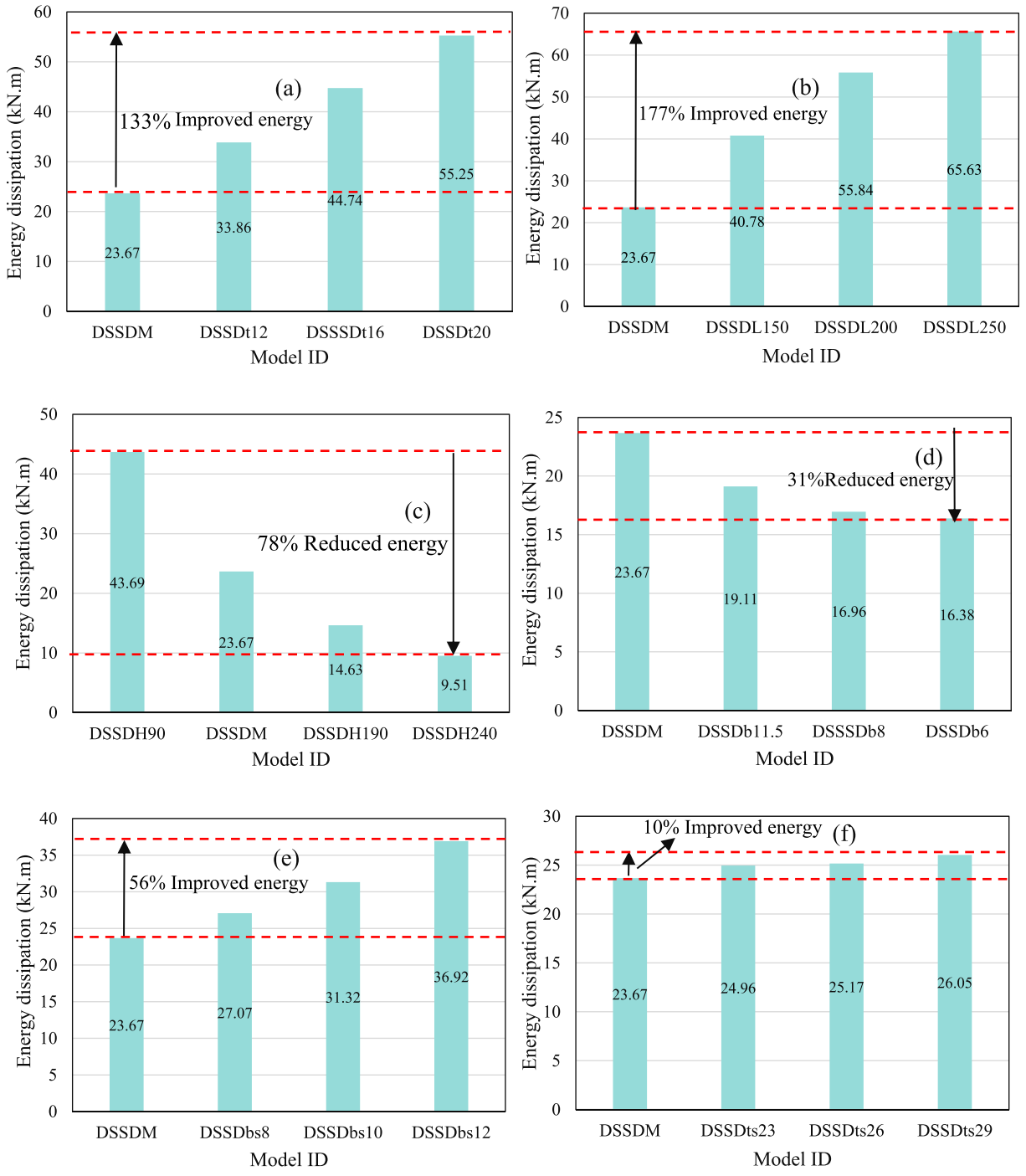

Fig. 16. Energy dissipation of DSSD with different: (a) thickness of slit plates t, (b) slit plates length L, (c) height of struts h, (d) struts width b, (e) stiffeners width b_s, and (f) stiffeners thickness t_s.

4.2. *Overstrength factor* Ω_0

The overstrength factor is relevant in capacity design, primarily as other structural members (e.g. brace members) should have a higher capacity than the DSSD to remain elastic, thus causing the damper to work as a "fuse" during earthquakes.

Fig. 18 shows the overstrength factor Ω_0 of the models (also listed in Table 2). In this figure, Ω_0 is defined as the ratio of the maximum strength to the yield strength of steel (Eq. (8)). The results indicate that the maximum strength of the new DSSD is higher than its yield strength (Eq. (8)) due to the hardening effect of steel. Overall, Ω_0 varies between 1.83 and 2.36, regardless of changes in

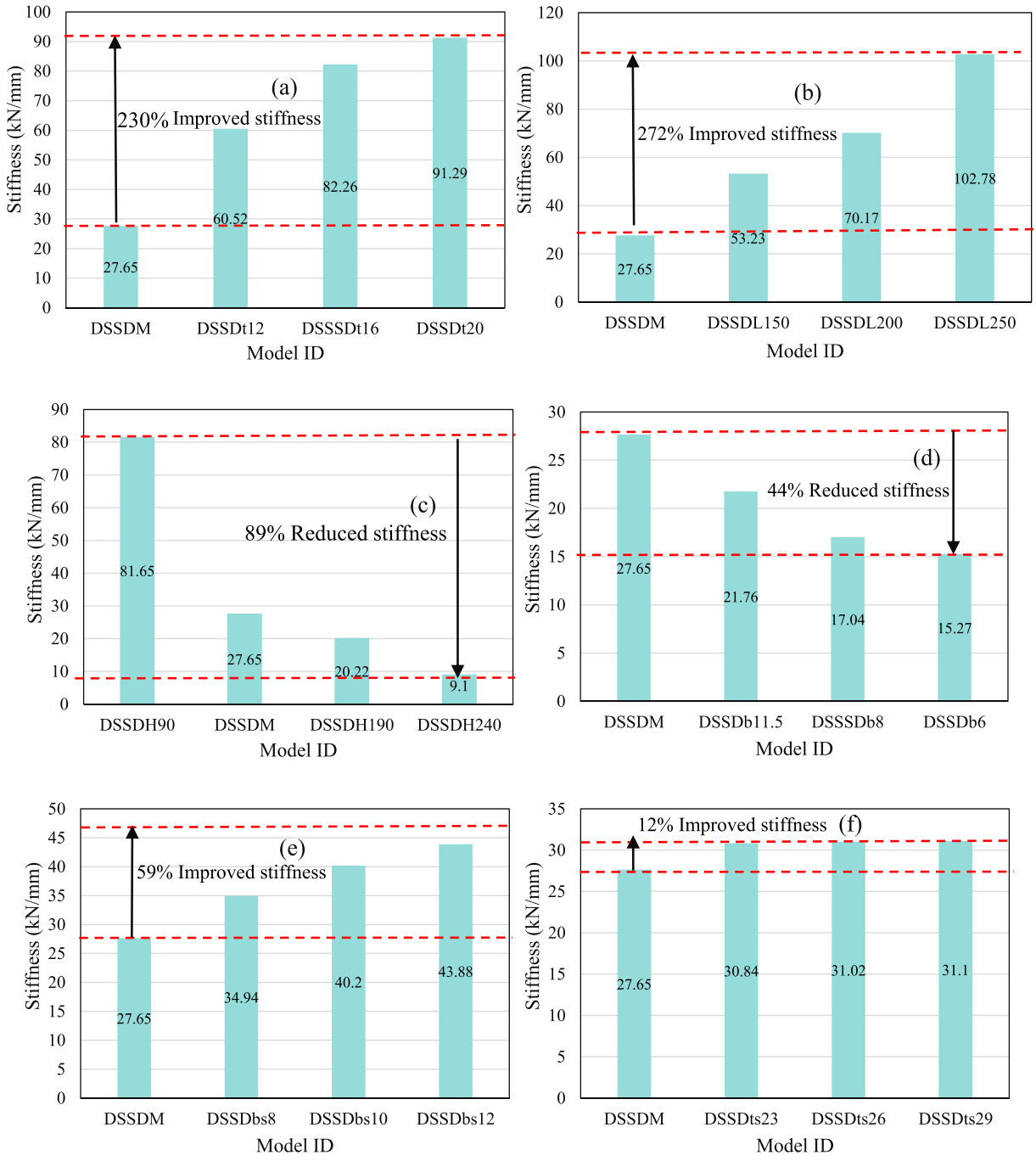

Fig. 17. Stiffness of DSSD with different: (a) thickness of slit plates t, (b) slit plates length L, (c) height of struts h, (d) struts width b, (e) stiffeners width b_s, and (f) stiffeners thickness t_s.

different geometrical parameters of the DSSD. The results in Fig. 18 show that Ω_0 increases only slightly with increasing values of L. For instance, increasing L from 100 mm (DSSDM) to 250 mm (DSSDL250) enhances Ω_0 by only 11%. However, increasing h (compare DSSDH90 vs DSSDH240) and b_s (DSSDM vs DSSDbs12) reduce Ω_0 by 21% and 14%, respectively. Note also that changes in t, t_s and b have a minor influence on Ω_0. Overall, the overstrength factors Ω_0 of the DSSD presented in Fig. 18 are consistent with values reported in past studies [35]. Until more data becomes available, it is recommended to adopt a value $\Omega_0 = 2.36$ for design purposes.

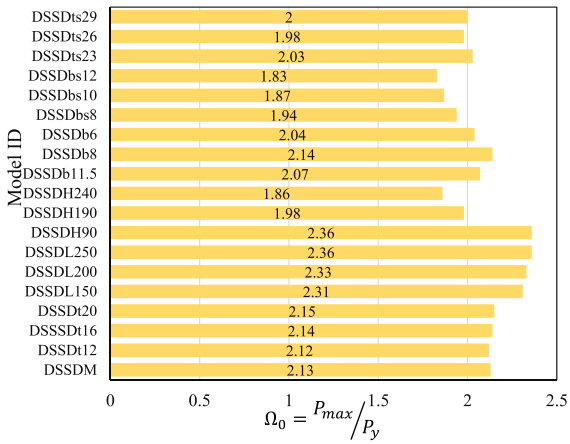

Fig. 18. Overstrength factor Ω_0 of DSSD models.

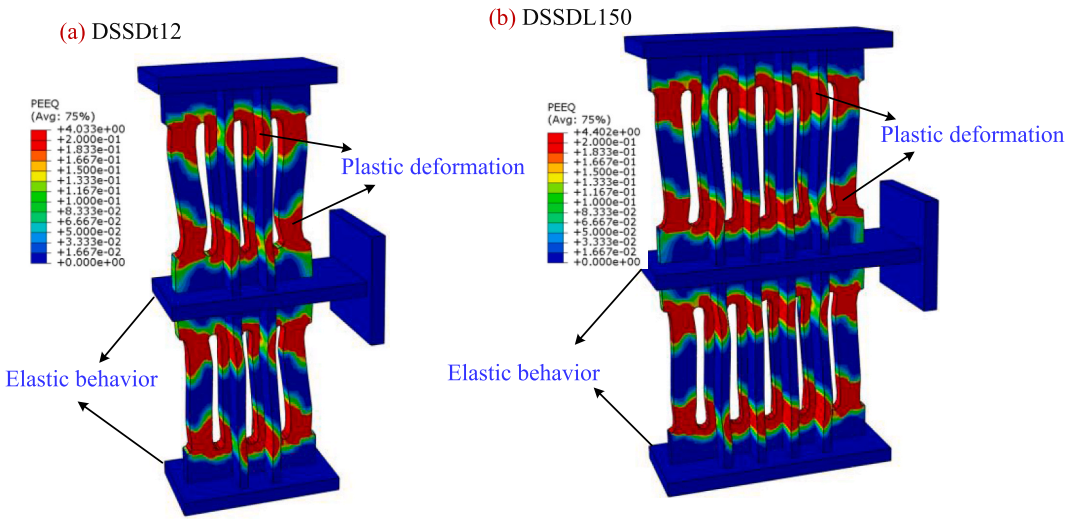

Fig. 19. PEEQ distributions of models: (a) DSSDt12, (b) DSSDL150.

4.3. PEEQ distribution

One of the design objectives of the DSSD is to concentrate the plastic behavior only in the slit plates and stiffeners (see Section 2). To verify this, Fig. 19 compares the PEEQ distribution of models DSSDt12 and DSSDL150, which are representative of other models listed in Table 2. The results show that, as intended, the slit plates and stiffeners have significant plastic deformations. On the other hand, there is no plastic demand in the middle plate and boundary plates (which remain elastic until the end of the numerical analyses), thus confirming the suitability of the design procedure.

5. Comparison between new DSSD and conventional slit damper

Figs. 20a–d compare the hysteresis curves and energy dissipation of the DSSD and a conventional slit damper [30,31]. Since the DSSDM model features similar slit plates to those in the experimental specimen DSSH2 [30,31], this specimen, as well as DSSDt12 and DSSDL150, were selected for comparison. The results in Figs. 20a–c indicate that DSSDM produces larger hysteresis loops than a conventional slit damper, which can be attributed to the use of the stiffeners and double slit plates. This results in an improvement in strength and energy dissipation capacity by up to 196.8% and 170.8%, respectively, compared to a conventional slit damper [30,31].

The maximum PEEQ value of the DSSD specimens is compared with the experimental benchmark value to assess the risk of damage of the DSSD. Fig. 21 illustrates the maximum PEEQ values of the DSSD models. The results show that all DSSD specimens exhibit lower PEEQ values compared to the benchmark value (PEEQ = 9.13). For instance, the maximum PEEQ value of the DSSDM model is 4.27 i.e. 65% lower than the benchmark value, which can be attributed to the use of stiffeners. It can also be seen that the parameters of the DSSD (except for *H*) do not significantly affect the PEEQ value. However, reducing *H* increases the PEEQ value, which can increase the

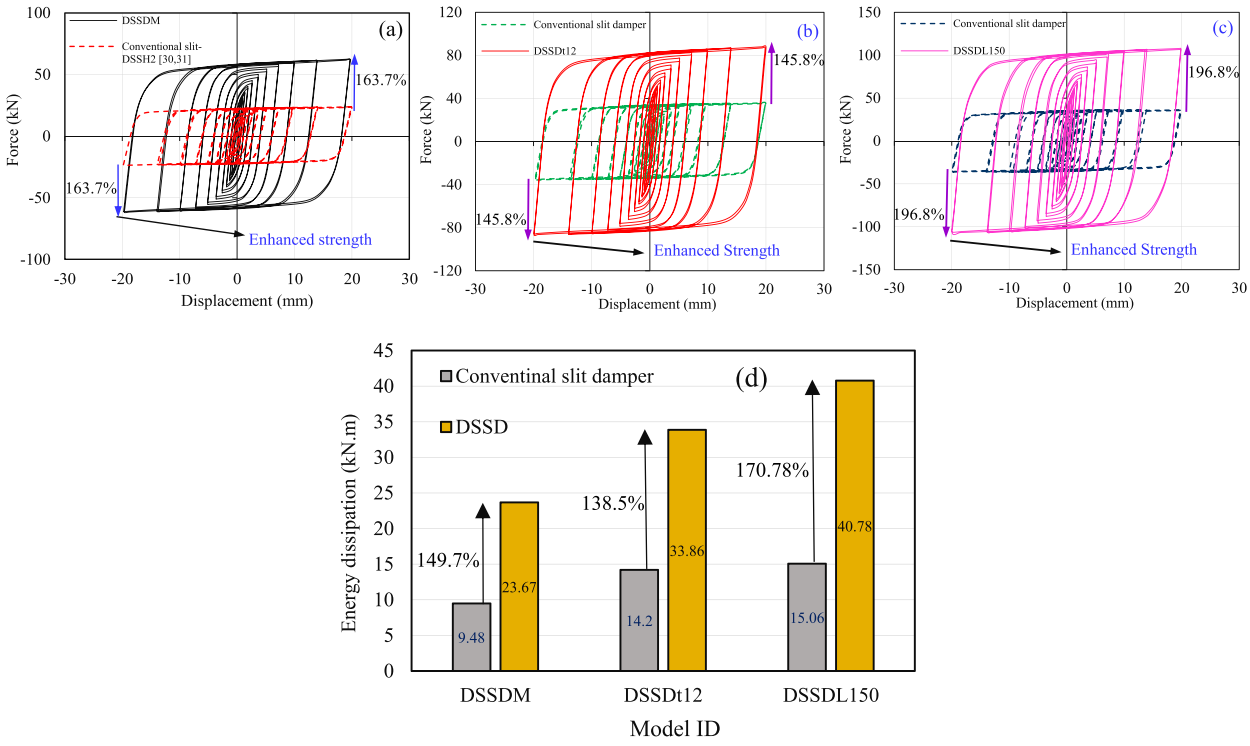

Fig. 20. Conventional slit damper vs DSSD: (a–c) hysteresis curve, (d) energy dissipation.

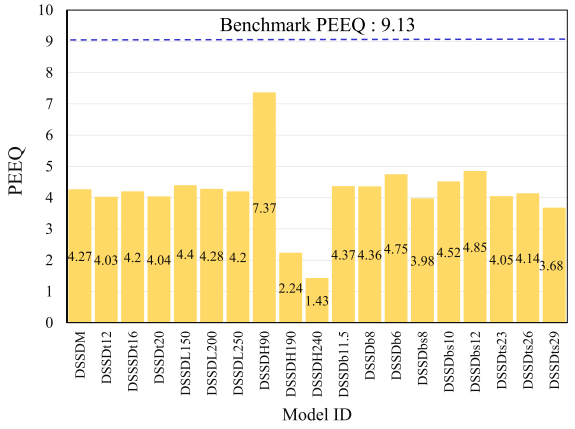

Fig. 21. Maximum PEEQ value of DSSD models.

Table 3
Details of brace models in Abaqus®.

Bare brace			Brace with DSSD						
ID	Length (mm)	Energy dissipation (kN·m)	Model	ID		Slit damper	Energy dissipation (kN·m)	Share of energy dissipation (%)	
								Brace	Damper
B400	4000	12.87	BD400	B400	+	DSSDt12	31.98	0.139	99.84
B450	4500	10.85	BD450	B450	+	DSSDt12	31.34	0.156	99.84
B500	5000	9.12	BD500	B500	+	DSSDM	22.86	0109	99.87
B550	5500	7.78	BD550	B550	+	DSSDH190	14.98	0.093	99.87

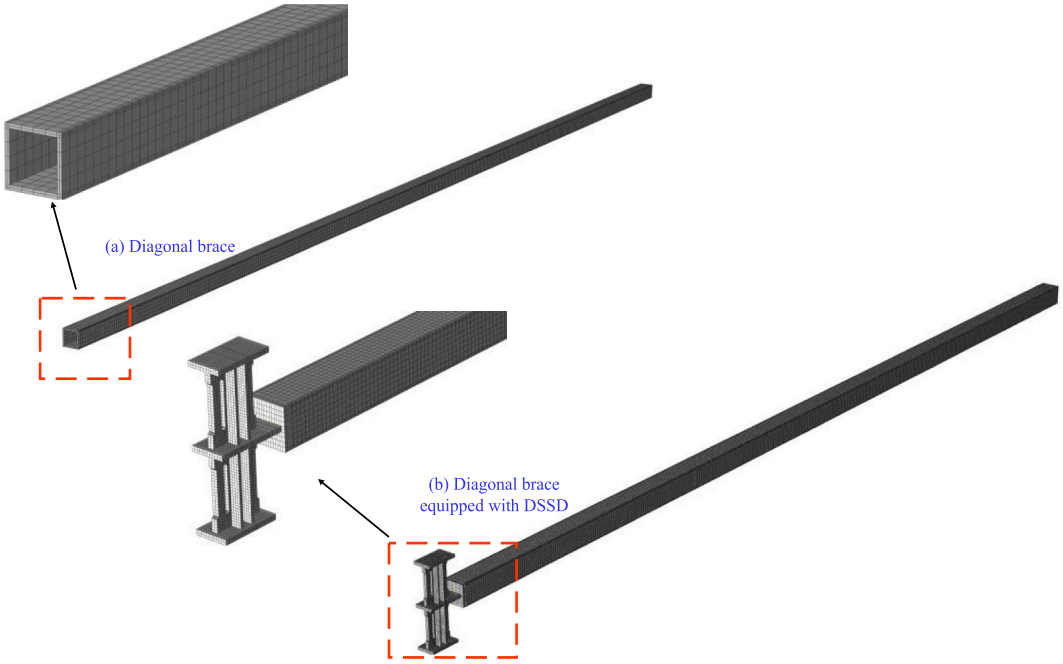

Fig. 22. Meshed model: (a) diagonal brace, and (b) diagonal brace with DSSD.

risk of damage. This observation agrees well with the damage reported by Nik-Hoosh and Kafi [30,31]. Overall, the results in Figs. 20 and 21 show that the new DSSD has the potential to improve energy dissipation capacity and delay failure compared to conventional slit dampers [30,31].

6. Hysteretic behavior of braces with DSSD

This section numerically analyzes the hysteretic behavior of the new DSSD together with a brace element of different lengths. Since a box-shaped brace was used in the calibration (see Fig. 10c), a box section with 50 mm width and 4 mm thickness is adopted here as the diagonal brace. The length of the diagonal brace is chosen to be either 4.0, 4.5, 5.0 or 5.5 m. These lengths are representative of a brace in a Chevron braced frame with a typical height of 3 m and spans of 5–7 m. The details of the brace models and main results (as discussed later) are given in Table 3. Fig. 22 shows the meshing of the models in Abaqus®. A similar modeling approach as that described in Section 3.1 (Stage 1) is adopted here for the brace. It should be noted that although a bolted connection was suggested for the DSSD, tie constraints were used as a reasonable simplification as proposed in past studies [10,56]. The brace models were analyzed under cyclic loading based on the loading protocol presented in Section 3.3. It should be noted that the DSDD and braces are chosen in such a way that the damper yields before the brace, by considering the damper's strength is close to compressive strength of the brace $\left(\frac{P_{design}}{\Phi P_n} = 0.90 \sim 0.95\right)$.

6.1. Hysteretic curves

Figs. 23a–d compare the hysteresis response of the diagonal braces and the braces with the DSSD, according to the models listed in Table 3. The results in Figs. 23a–d show that, as expected, buckling of the brace under compressive loads leads to an asymmetric and unstable hysteretic response of the brace models B400, B450, B500 and B550. The tensile and compressive strength of the diagonal braces reduce after tensile yielding and buckling occur, respectively, thus showing some strength degradation. Failure of the brace models is dominated by buckling of the braces. In contrast, the addition of the new DSSD to the braces leads to symmetric and stable hysteretic response in tension and compression (see models BD400, BD450, BD500 and BD550 in Fig. 23a–d). In these models, the strength of the braces with DSSD increases after yielding due to the damper's overstrength. The results suggest that the braces with the DSSD develop large symmetric hysteresis loops, which in turn lead to ductile behavior (due to damper yielding). It should be noted that the brace with DSSD (Fig. 23a) exhibits higher tension than compression forces. This phenomenon can be attributed to geometric nonlinearity and large deformations, as reported previously by Rodríguez-Moreno et al. [47].

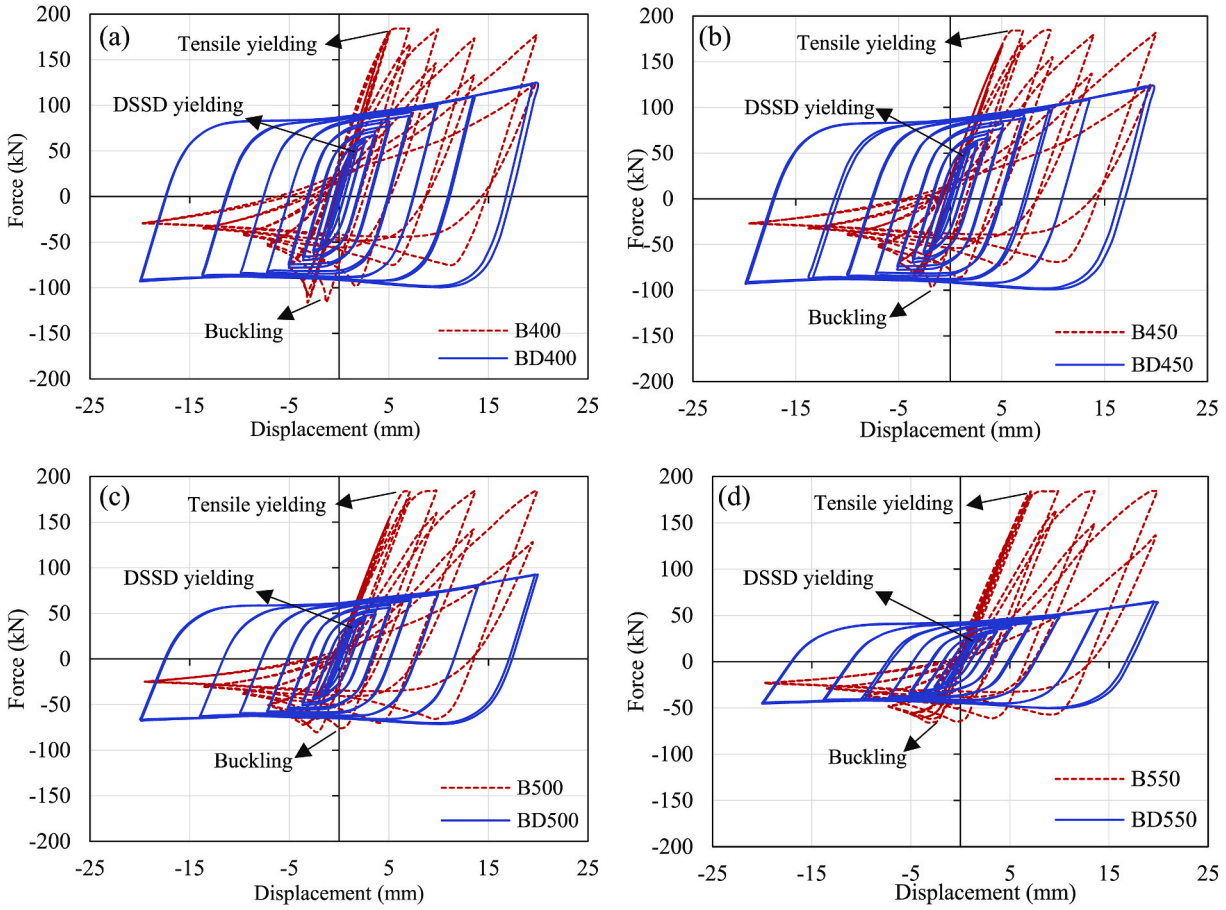

Fig. 23. Cyclic response models: (a) B400 vs BD400, (b) B450 vs BD450, (c) B500 vs BD500, (d) B550 vs BD550.

6.2. Strength degradation

Strength degradation is a significant factor in evaluating the hysteresis response of elements [57]. The following equation defines a degradation factor (λ_i) to quantify the strength degradation of a hysteresis curve [57]:

$$\lambda_i = \frac{P^i_{max,j}}{P^{i-1}_{max,j}} \tag{9}$$

where $P^i_{max,j}$ and $P^{i-1}_{max,j}$ are the maximum loads under the $(i)^{th}$ and $(i-1)^{th}$cycles, respectively, corresponding to the j^{th}loading displacement. A value $\lambda_i \geq 1$ in the above equation implies that there is no strength degradation in the hysteresis curve.

Figs. 24a-d compare the strength degradation curves of the brace models (see Table 3) as a function of displacement, as calculated by Abaqus®. The results indicate that the values λ_i for braces with DSSD (BD400, BD450, BD500 and BD550) are always higher than 1 during loading, thus showing no strength degradation. Conversely, the bare braces (B400, B450, B500 and B550) have $\lambda_i < 1$ in the negative displacement direction (i.e. compressive loads), which suggests some strength degradation occurs due to buckling of the brace. At a common negative displacement of 14 mm, the λ_i values of models BD400, BD450, BD500 and BD550 are 38%, 23%, 15% and 14% higher than their corresponding bare brace, indicating the desirable performance of CBFs with DSSD.

6.3. Energy dissipation

Energy dissipation capacity is widely regarded as an important indicator of seismic performance [10,13]. In this study, the energy dissipation is calculated as the area inside the hysteresis loops shown in Figs. 23a-d. Table 3 summarizes the energy dissipated by the analyzed models. As expected, the braces with the new DSSD have higher energy dissipation capacity than the bare braces. Indeed, models BD400, BD450, BD500 and BD550 have 148%, 189%, 151% and 92% higher energy dissipation, respectively, compared to the bare brace models. This confirms that braces with the new proposed DSSD can dissipate more energy during earthquakes. It should be noted that, for an enhanced performance, low-yield point (LYP) steel could be used in design. As such, LYP steel could offer superior

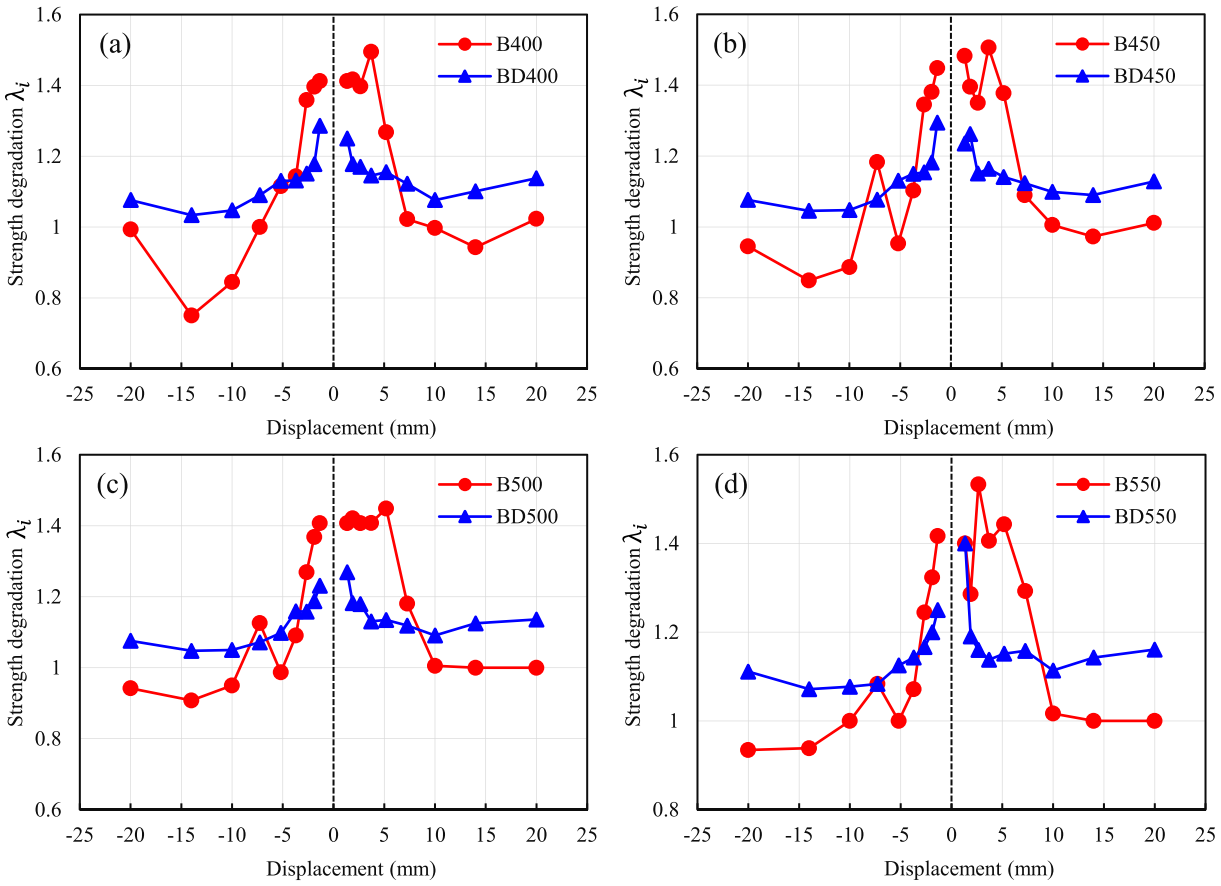

Fig. 24. Strength degradation curves of braces: (a) B400 and BD400, (b) B450 and BD450, (c) B500 and BD500, (d) B550 and BD550.

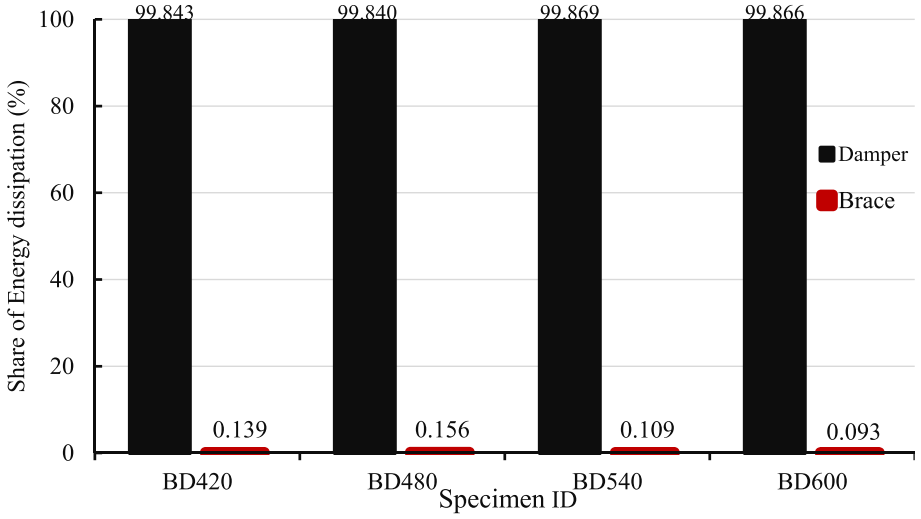

Fig. 25. Dissipated energy by brace and DSSD in models.

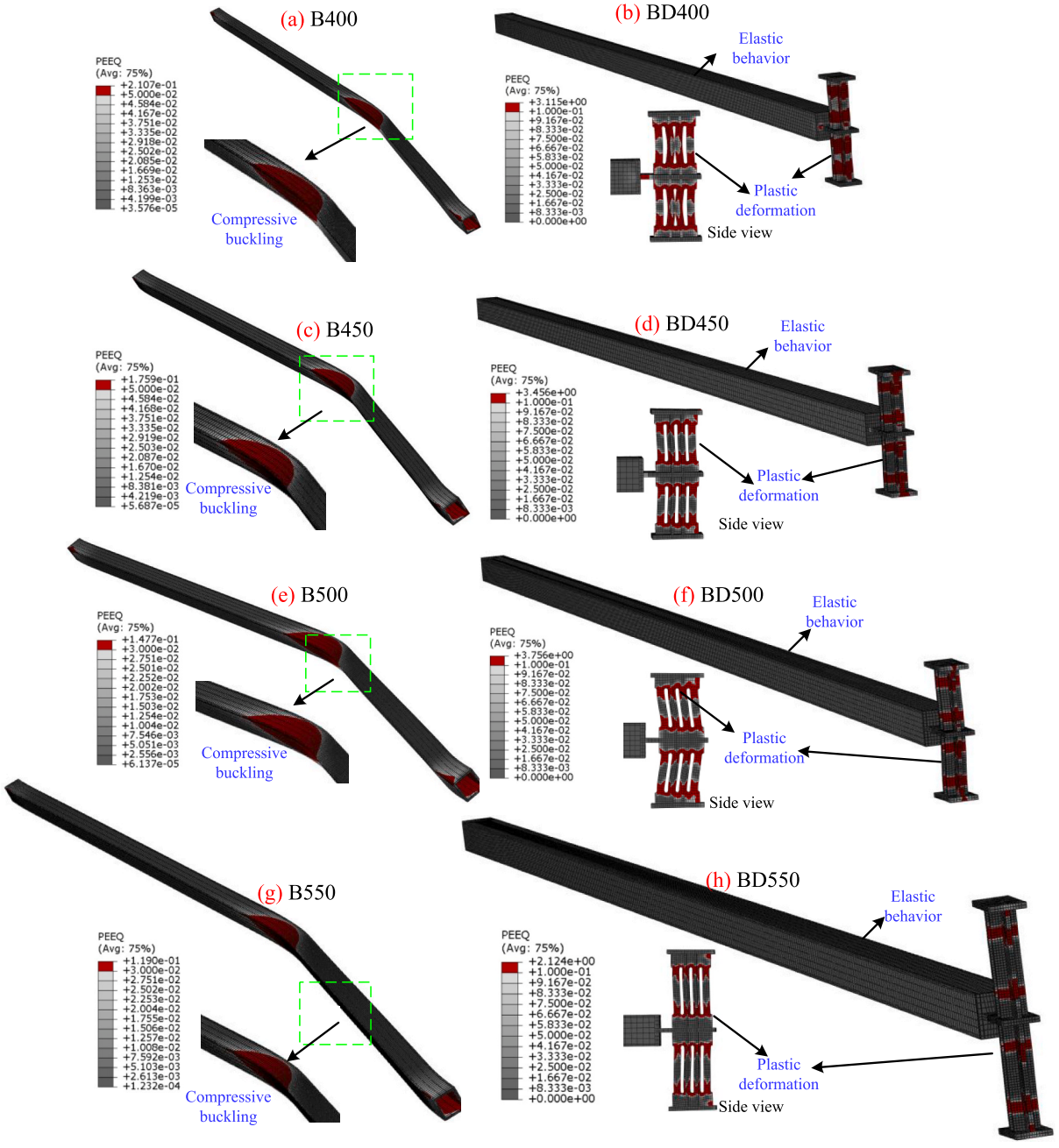

Fig. 26. PEEQ in models: (a) B400, (b) BD400, (c) B450, (d) BD450, (e) B500, (f) BDL500, (g) B550, (h) BD550.

energy dissipation capability under cyclic loading, thereby improving the effectiveness of dampers in seismic applications. This finding has been confirmed in previous studies [35,58].

In the proposed design method, the DSSD is expected to work as a seismic "fuse". Hence, the brace element should not dissipate energy. Fig. 25 compares the amount of energy dissipated by the brace and DSSD of models BD400, BD450, BD500 and BD550, as obtained from Abaqus®. The results in Fig. 25 indicate that, in all models, the proposed DSSD dissipates over 99% of the total energy, which confirms that the DSSD works as a "fuse". The amount of energy dissipated by the braces (<1% of the total energy) indicates that the braces remain elastic during the analyses, as intended in the design methodology. Overall, the energy dissipation results presented in Table 3 and Fig. 25 are consistent with previous studies that examined the effect of dampers on braces [10,13,56].

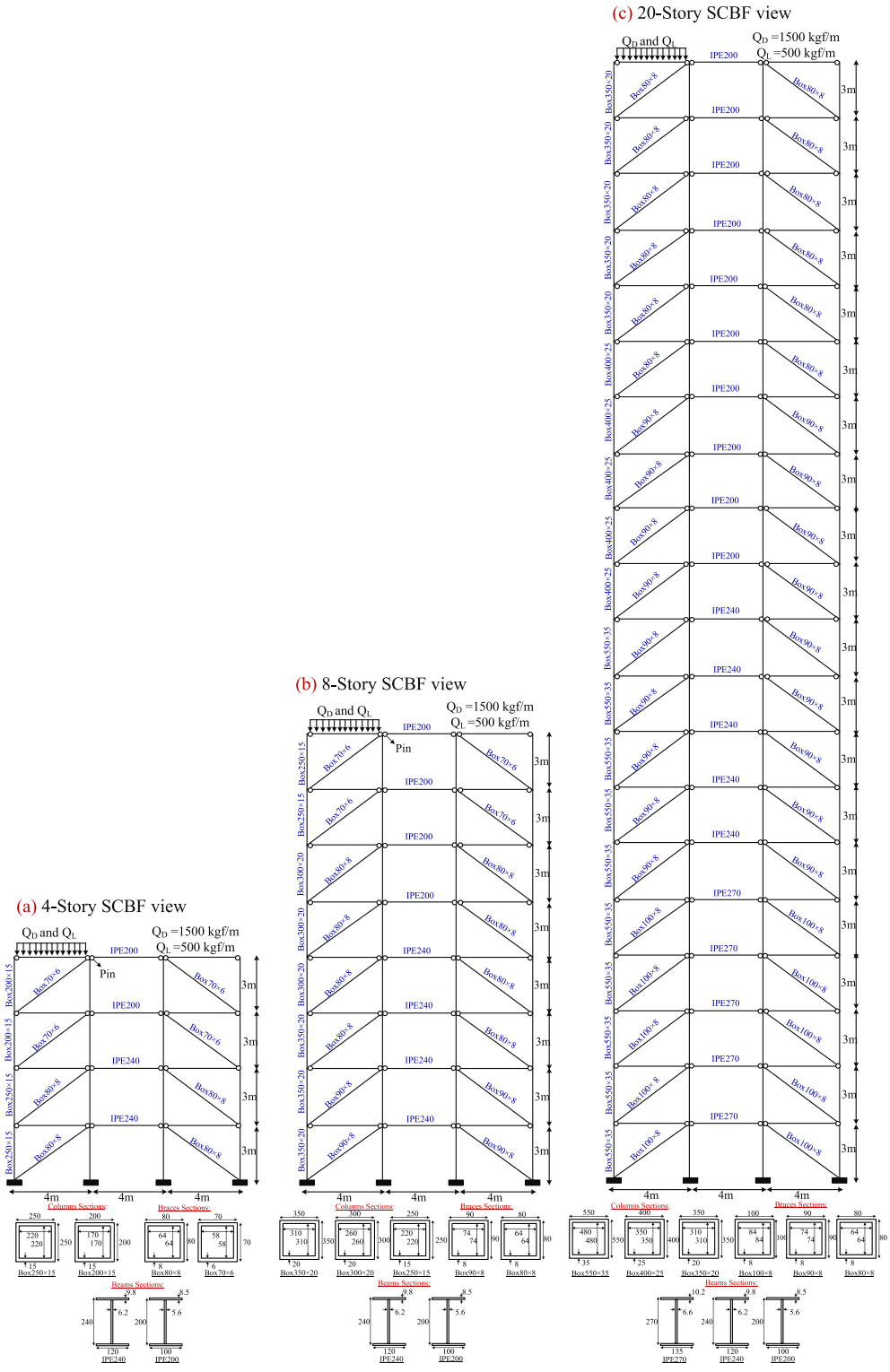

Fig. 27. Properties of the case study frames: (a) 4-story SCBF, (b) 8-story SCBF, (c) 20-story SCBF.

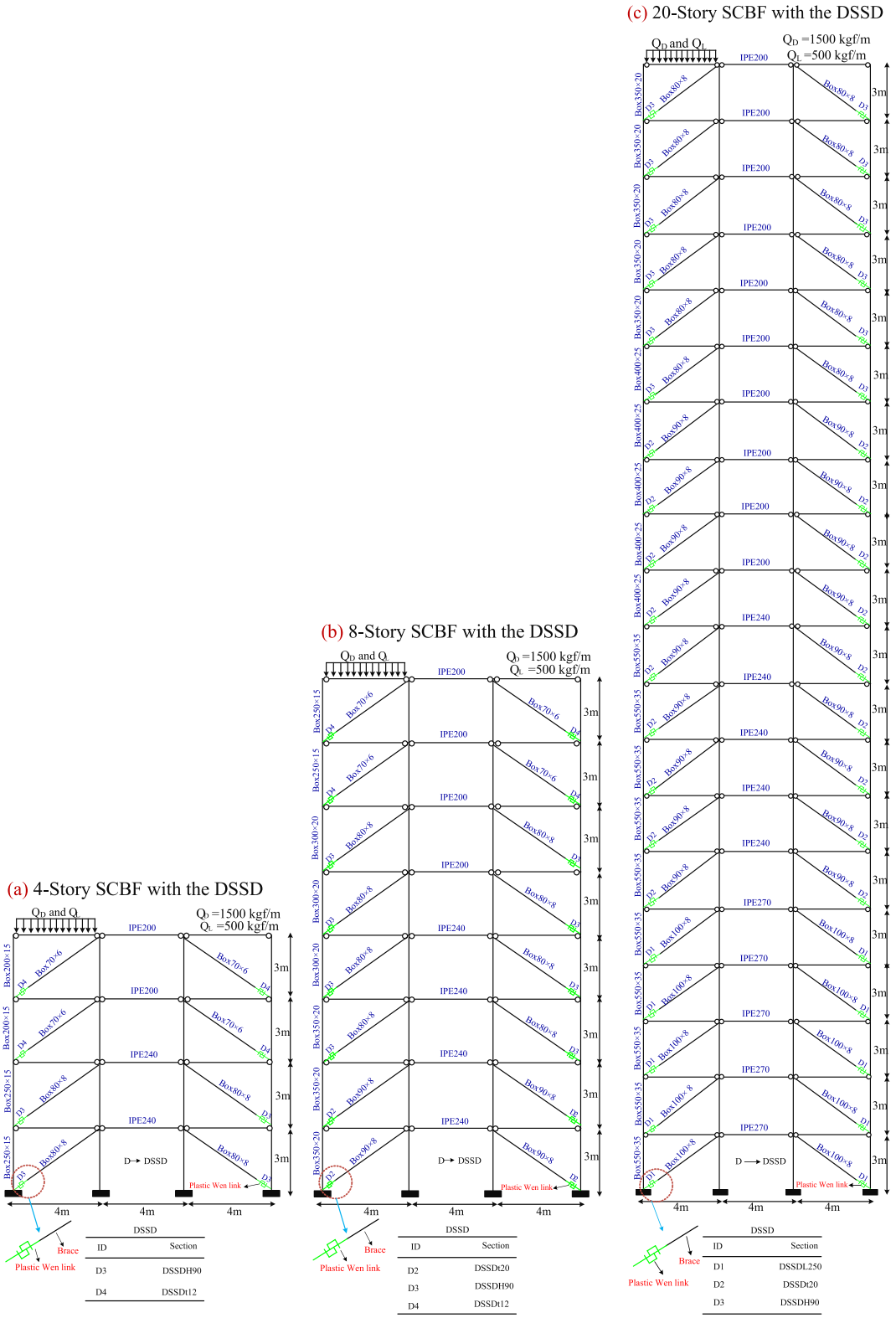

Fig. 28. Properties of braced frames with DSSD: (a) 4-story SCBF, (b) 8-story SCBF, (c) 20-story SCBF.

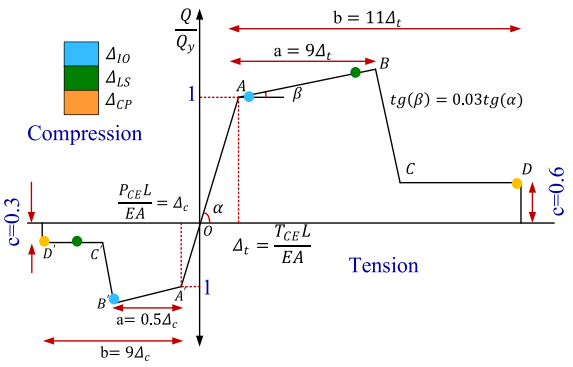

Fig. 29. Force-deformation curve for bracing members based on ASCE/SEI 41-13 [61].

6.4. PEEQ distribution

The distributions of PEEQ in the brace models are presented in Figs. 26a–h. In these figures, PEEQ values higher than zero imply the presence of damage. Figs. 26a–c, e and g show that the bare braces (models B400, B450, B500 and B550) experience buckling and plastic strains. At the buckled region, the braces have values of PEEQ of 0.1–0.2. On the other hand, the results in Figs. 26b–d, f and h show zero PEEQ in the braces of models BD400, BD450, BD500 and BD550, whereas the DSDD have PEEQ values between 2 and 4. It can be concluded that the DSSD can effectively shift the failure mode of the brace from compressive buckling to yielding of the damper.

7. Seismic behavior of SCBF buildings with DSSD

7.1. Geometry and design considerations of case study structures

To evaluate the effectiveness of the new DSSD at improving the seismic performance of steel buildings, 4, 8 and 20-story Special Concentric Braced Frames (SCBFs) with and without DSSDs are subjected to time-history analysis. The bare SCBFs (see Figs. 27a–c) are 2D regular frames with three spans of length of 4 m, and with a constant story height of 3 m. For design purposes, these SCBFs were considered as residential buildings located in a high seismic region with a peak ground acceleration (PGA) of 0.35g, in accordance with the Iranian seismic code [59]. A soil type II (375 m/s $\leq V_s \leq$ 750 m/s) is considered in the design, according to the same code [59]. The SCBFs are modeled in SAP2000® [60] assuming that the ground floor columns are fixed to the ground. A combination of uniform distributed dead loads (Q_D) and live loads (Q_L) is applied on the beams. The upper limit of the gravity load ($1.1[Q_D + 0.2Q_L]$) is employed in the analysis [61]. Moreover, the floors are considered as rigid diaphragms. Pinned connections are used for all beam-to-column connections. All structural members (beams, columns and braces) are designed according to AISC 360-16 [49] and to the Iranian seismic code [59]. The final cross sections of the members, as provided by SAP2000®, are given in Figs. 27a–c. Likewise, two counterpart SCBFs with the new DSSD located at the outermost spans are also analyzed (see Figs. 28a–c), assuming that the DSSDs were placed at the bottom end of the braces. It should be noted that, in Figs. 28a–c, the DSSD are chosen in such a way that the damper yields before the brace by considering that the damper's strength is close to compressive strength of the brace i.e. considering that

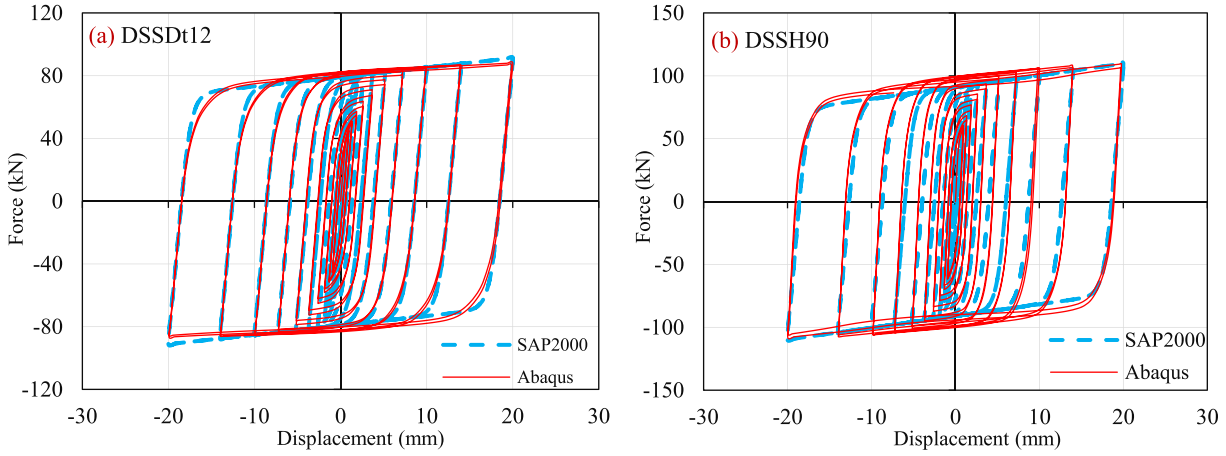

Fig. 30. DSSD modeled with SAP2000® and Abaqus®: (a) DSSDt12, and (b) DSSDH90.

Table 4
Records for time history analyses.

ID	Earthquake, year	Station	Epicentral distance (km)	PGA (g)	M_w
R1	Imperial Valley, 1979	El Centro Array	29.4	0.38	6.5
R2	Loma Prieta, 1989	Gilroy Array	31.4	0.56	6.9
R3	Loma Prieta, 1989	Capitola	9.80	0.53	6.9
R4	Friuli (Italy), 1976	Tolmezzo	20.2	0.35	6.5
R5	Kocaeli (Turkey), 1999	Duzce	98.2	0.36	7.5
R6	Hector Mine, 1999	Hector	26.5	0.34	7.1
R7	Northridge, 1994	Beverly hills	13.3	0.52	6.7
R8	Northridge, 1994	Canyon Country	26.5	0.48	6.7
R9	Manjil, 1990	Abbar	40.4	0.51	7.4

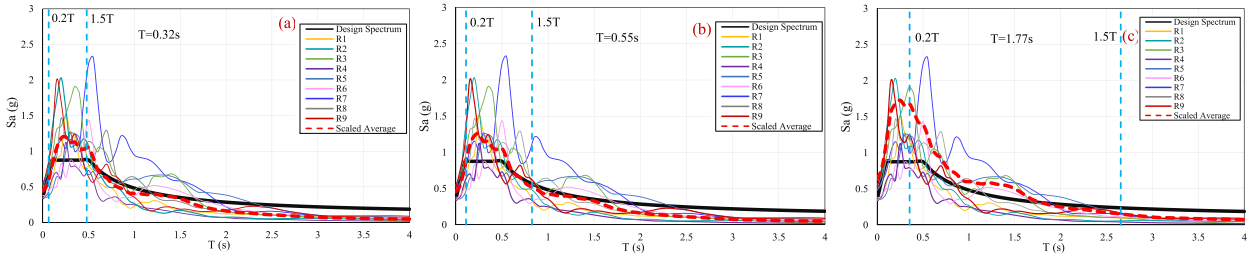

Fig. 31. Acceleration response spectra for nine selected records: (a) 4-story frame, (b) 8-story frame, (c) 20-story frame.

Table 5
Maximum base shear of SCBFs (kN).

ID	4-story SCBF			8-story SCBF			20-story SCBF		
	Bare	with DSSD	Reduction (%)	Bare	with DSSD	Reduction (%)	Bare	with DSSD	Reduction (%)
R1	378.8	187.6	50.5	581.2	288.1	50.4	681.9	409.1	40.0
R2	775.5	274.1	64.7	926.6	408.4	55.9	1019.8	652.1	36.1
R3	741.1	235.9	68.2	808.8	322.4	60.1	1389.3	724.8	47.8
R4	673.8	239.1	64.5	776.2	362.5	53.3	1232.4	628.4	49.1
R5	476.7	213.5	55.2	628.3	311.5	50.4	1602.5	660.9	58.8
R6	740.8	274.8	62.9	828.8	337.0	59.3	1261.1	583.6	53.7
R7	327.4	208.7	36.3	833.4	349.9	58.0	1042.4	399.4	61.7
R8	335.4	190.0	43.4	445.9	203.0	54.5	436.1	321.6	26.3
R9	319.3	189.7	40.6	479.8	298.3	37.8	1166.6	751.5	35.6
Average	**529.9**	**223.7**	**57.8**	**701.0**	**320.1**	**54.3**	**1092.5**	**570.2**	**47.8**

$\frac{P_{design}}{\Phi P_n} = 0.90 \sim 0.95$.

7.2. Material properties

The beams of the case study frames are modeled as elastic elements. The nonlinear behavior of the columns and braces is modeled using concentrated plastic hinges at critical zones. As such, P-M3 plastic hinges were assigned at the top and bottom of all columns [60]. The properties of the plastic hinges are defined in accordance with ASCE/SEI 41-13 [61]. In the SCBF, the bracing members dissipate seismic energy through axial deformation. Hence, the axial behavior of the braces was modeled utilizing an axial hinge located at the midspan of the braces. Fig. 29 shows the properties of the bracings' hinges, as determined using ASCE/SEI 41-13 [61]. In this figure, T_{CE} and P_{CE} are the expected tensile strength and expected compressive strength, respectively; L is the length of the brace; A is the cross-section area of the brace; and E is the modulus of elasticity. The parameters a, b and c in Fig. 29 are defined based on ASCE/SEI 41-13.

The DSSD was modeled as a nonlinear Plastic Wen link element, which has been effectively used to model metallic dampers in past studies [62,63]. It should be noted that the DSSDs are selected so that they yield before the bracing elements. To validate the hysteretic response of the new DSSD in SAP2000®, two models (DSSDt20 and DSSDH90) are modeled in SAP2000® and then subjected to cyclic load. Figs. 30a–b compare the hysteresis curves (force-displacement) results obtained from SAP2000® and Abaqus®. It is shown that the hysteresis curves obtained by SAP2000® match well the Abaqus® results, thus confirming that the Plastic Wen link element can simulate well the behavior of the new DSSD. The minor differences in the predictions can be attributed to differences in the modeling approaches adopted in the two pieces of software.

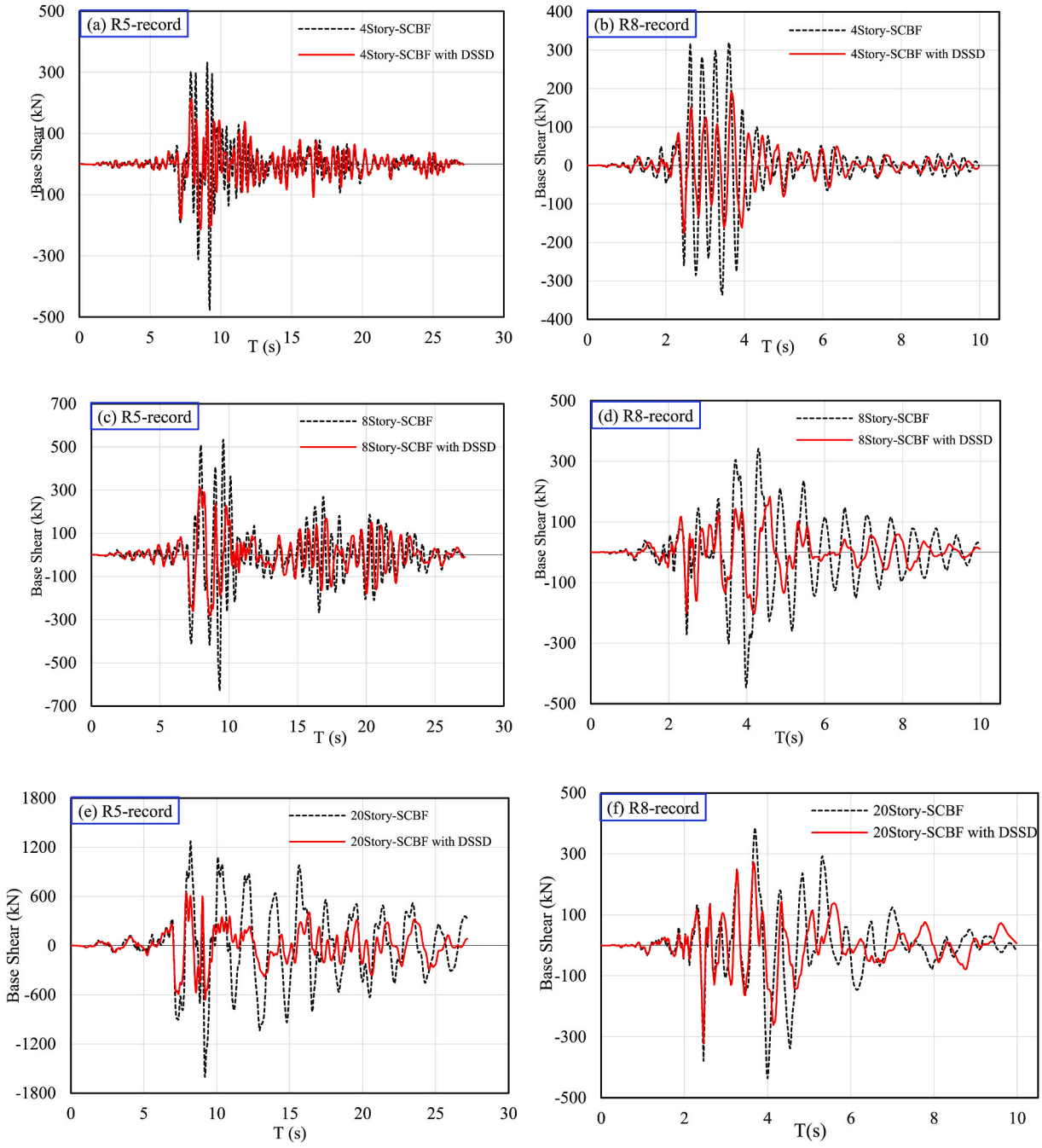

Fig. 32. Base shear time histories of SCBFs with and without DSSDs: (a)–(b): 4-story frame, (c)–(d): 8-storyframe, and (e)–(f) 20-story frame.

7.3. Ground motion records

Nine far-field earthquake records are selected from FEMA P695 [64] to perform nonlinear time-history analyses (see Table 4). All records are scaled according to the Iranian seismic code [59]. Accordingly, the acceleration spectrum was first obtained for all records, and then the records were scaled so that the average of the acceleration spectra was higher than design spectrum in a period range from $0.2T$ to $1.5T$, where T is the fundamental period of the building. Fig. 31 shows the scaled acceleration spectra for the earthquake records in Table 4, as well as the fundamental periods of the 4, 8 and 20-story frames.

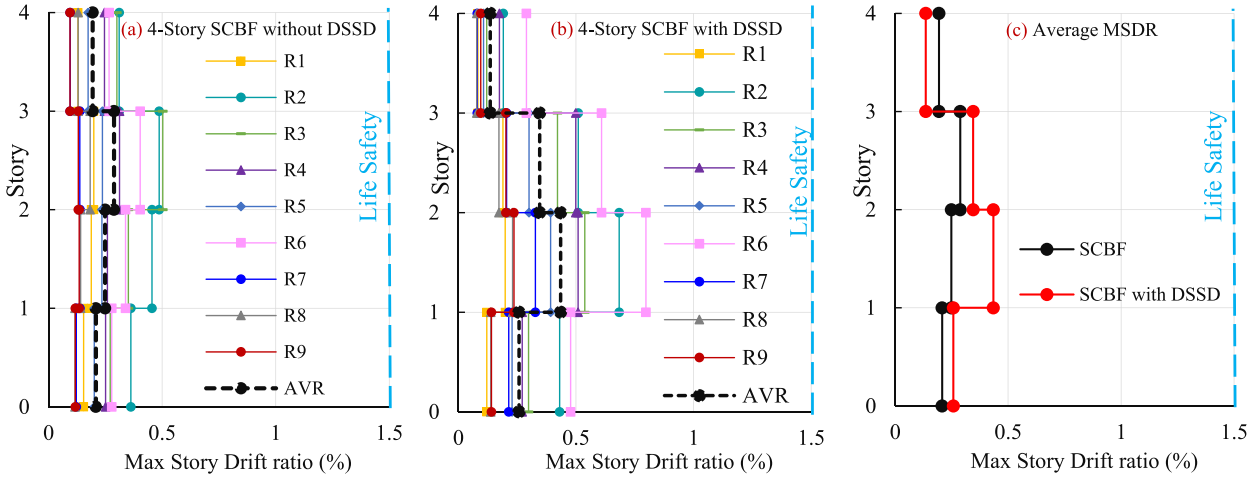

Fig. 33. MSDR of 4-story SCBFs subjected to records: (a) without DSSD, (b) with DSSD, (c) average MSDR.

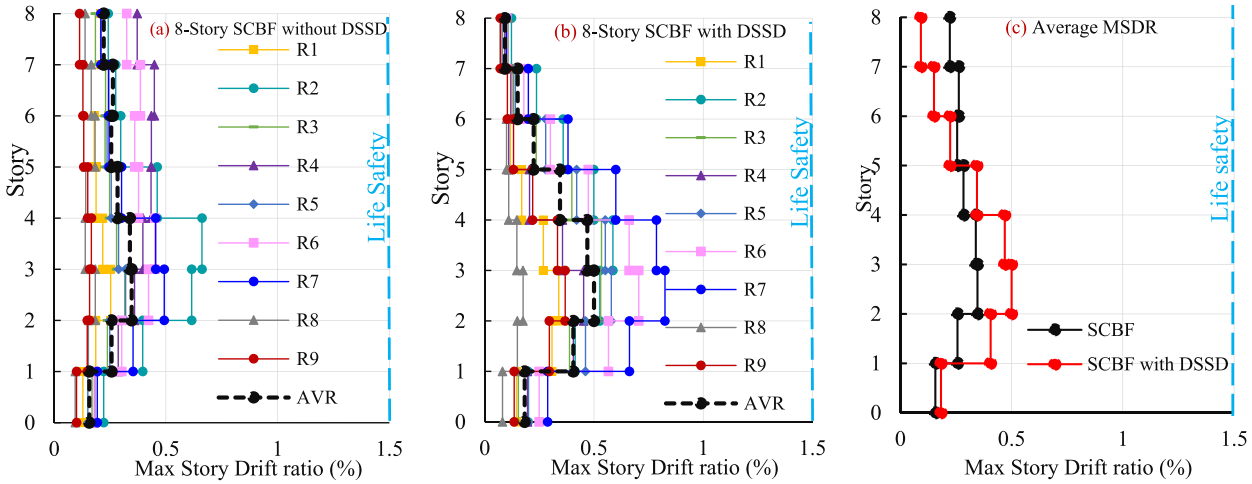

Fig. 34. Maximum story drift ratios of the 8-story SCBFs under earthquake records: (a) without DSSD, (b) with DSSD, (c) average MSDR.

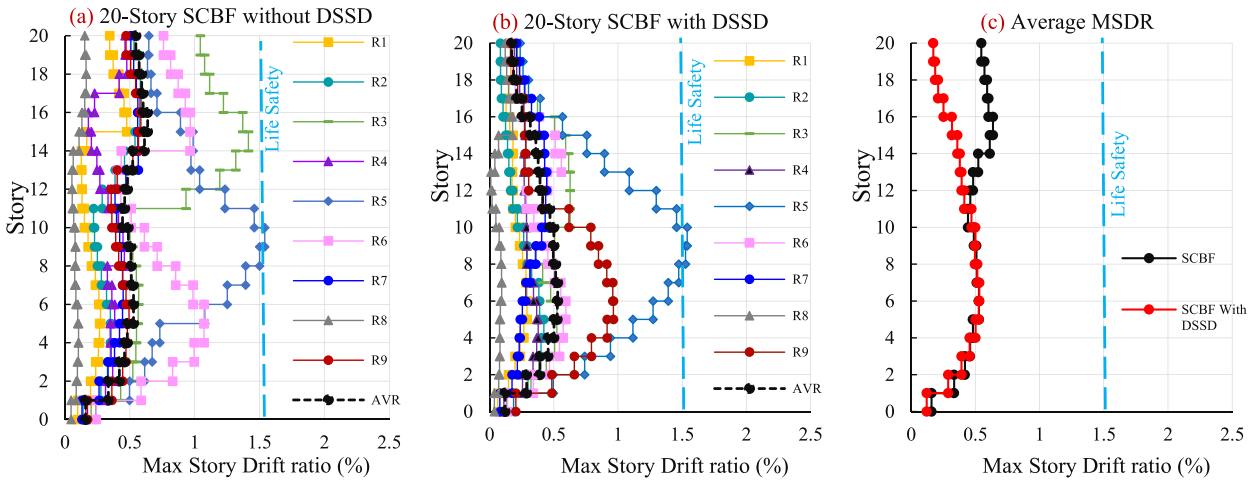

Fig. 35. Maximum story drift ratios of the 20-story SCBFs under earthquake records: (a) without DSSD, (b) with DSSD, (c) average MSDR.

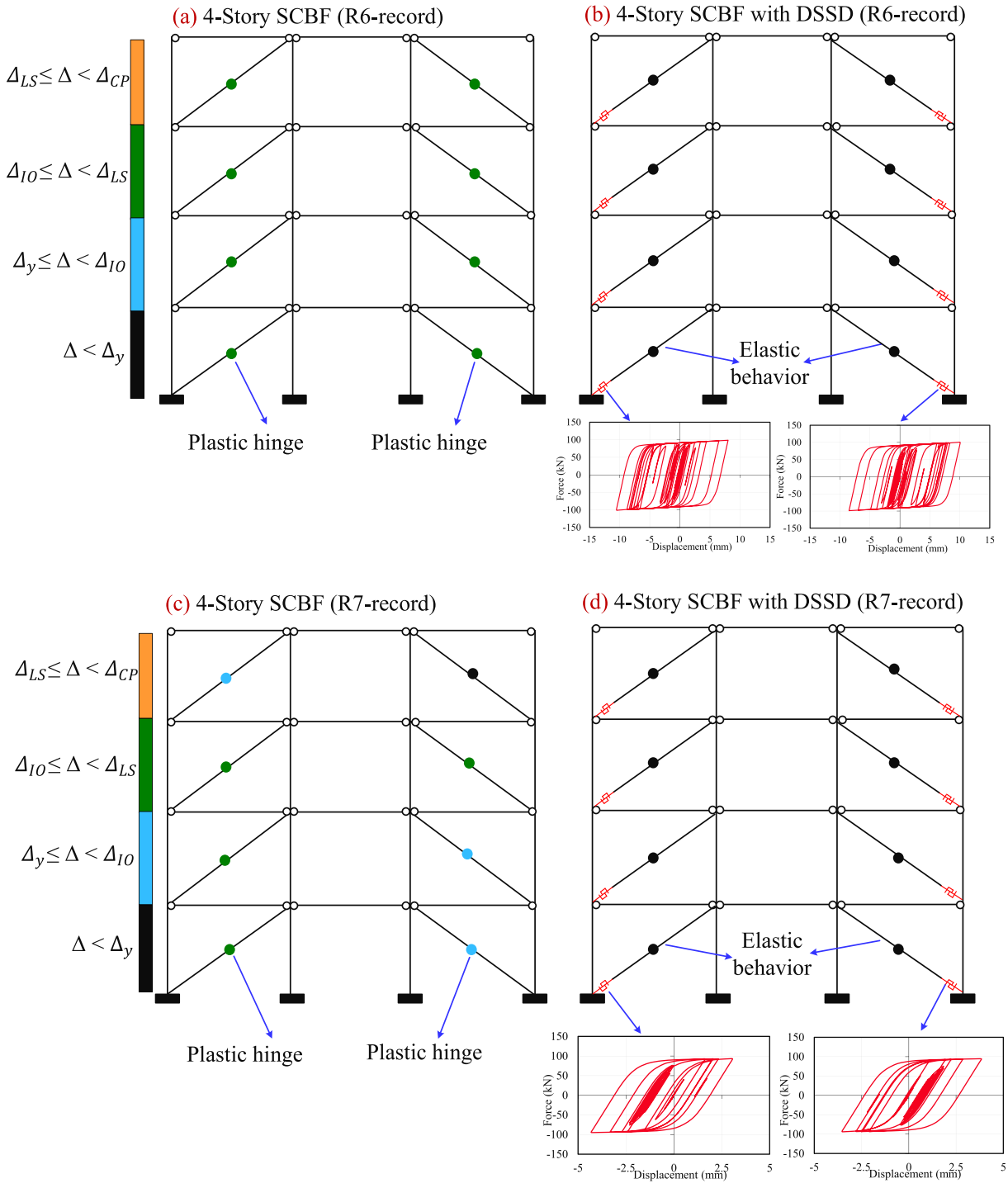

Fig. 36. Plastic hinging of 4-story SCBFs with and without DSSD: (a)–(b) record R6, and (c)–(d) record R7.

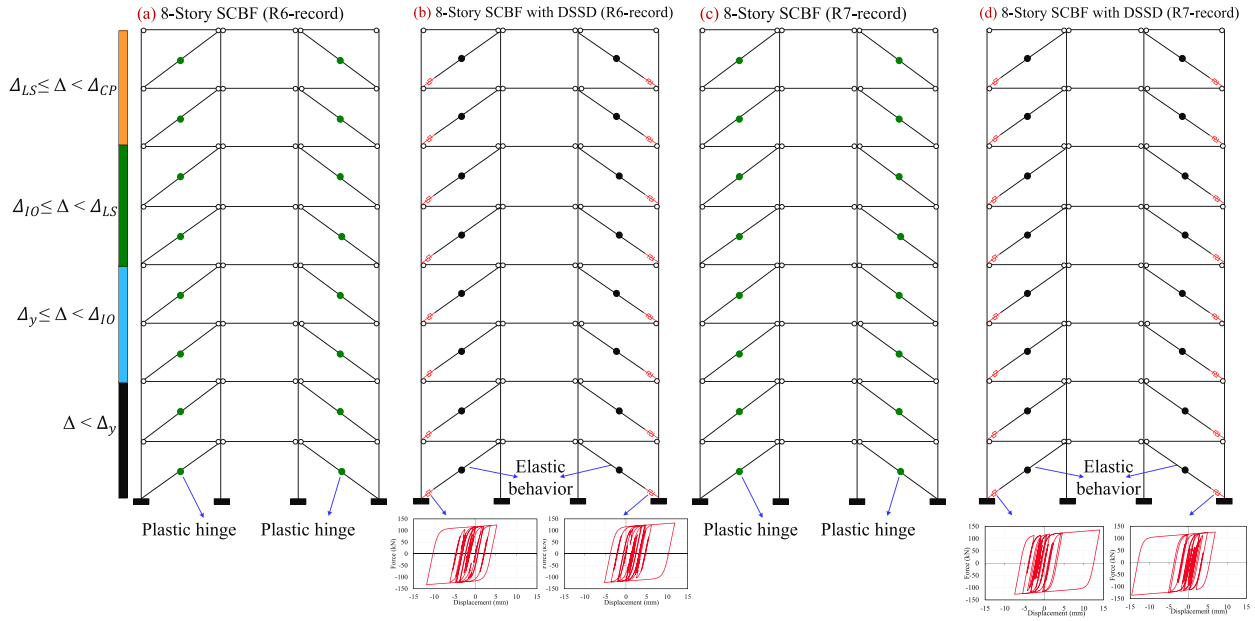

Fig. 37. Plastic hinging of 8-story SCBFs with and without DSSD: (a)–(b) record R6, and (c)–(d) record R7.

7.4. Nonlinear time history analysis results

a) Base shear. Figs. 32a–f compare the base shear of the SCBFs with and without the new DSSD for records R5 and R8. The results from these records are representative of other records used in the analysis. It can be observed that the base shear significantly decreased in the models with the new DSSD. Table 5 summarizes the maximum base shear of the SCBFs subjected to the earthquake records. The results confirm that the DSSD reduced the maximum base shear of the 4, 8 and 20-story SCBFs between 36.2%–68.2%, 37.8%–60.1% and 26.3%–61.7%, respectively. Overall, the use of the new DSSDs reduced the maximum base shear by 57.8%, 54.3% and 47.8% in the 4, 8 and 20-story SCBFs, respectively.

b) Maximum drifts. Maximum Story Drift Ratio (MSDR) are indicative of the performance level of a structure [65–68]. Figs. 33a–c, Figs. 34a–c and Figs. 35a–c compare, respectively, the MSDR of the 4-story, 8-story and 20-story SCBFs subjected to the earthquakes. The results in Figs. 33a–c indicate that the use of DSSDs generally increased the MSDR in the first and second stories, which can be attributed to the reduction of the original lateral stiffness of the system [10], leading to a longer fundamental period of the structure. The results in Figs. 34a–c and Figs. 35a–c show similar trends for the 8 and 20-story SCBF, where the DSSD increased the MSDR in the lower stories but reduced it in the upper stories. Despite this, the 4, 8 and 20-story SCBFs with DSSDs all satisfy the Life Safety performance level (MSDR = 1.5%), as suggested in FEMA 356 [69].

c) Plastic deformations. Figs. 36a–d, Figs. 37a–d and Figs. 38a–d shows, respectively, the local damage in the 4, 8 and 20-story SCBFs with and without DSSDs subjected to records R6 and R7. The results from these records are representative of other records used in the analysis. It is shown that the bare SCBFs experience plastic hinging at the braces. According to ASCE 41-13 [61], plastic hinges in the 4 and 8-story SCBFs satisfy the Life Safety performance level, while most hinges in the 20-story SCBFs meet the Collapse Prevention performance level (see Fig. 29). However, the braces of the SCBFs with DSSDs remain elastic (OA and OA' regions in Fig. 29), whereas only the DSSDs dissipate energy through hysteretic behavior. The hysteresis curves shown in Figs. 36–38b and d confirm the stable and symmetric behavior of the DSSDs when the buildings are subjected to the earthquake records. The findings also suggest that the new DSSD can effectively prevent damage to the braces, thereby acting as a structural "fuse" during strong shaking.

8. Comparison of BRB frame and SCBF with DSSD

BRBs have been widely proposed to improve the seismic performance of structures [15,16]. This section compares the seismic performance of BRB frames (BRBFs) vs SCBFs fitted with DSSDs. Only the 4-story and 8-story models are considered here. For a fair comparison, the BRBs and DSSDs are assumed to have similar yield strength and stiffness. A Plastic-Wen link element was used for modeling in SAP2000® as such element can accurately predict the behavior of metallic dampers [60,62,63]. To validate the hysteretic response of the BRB model, Specimen 99-1 from a PEER report was used [70]. Fig. 39 compares the experimental and numerical hysteresis curves (force-displacement). The SAP2000® results show good agreement with experimental data [70], confirming that the

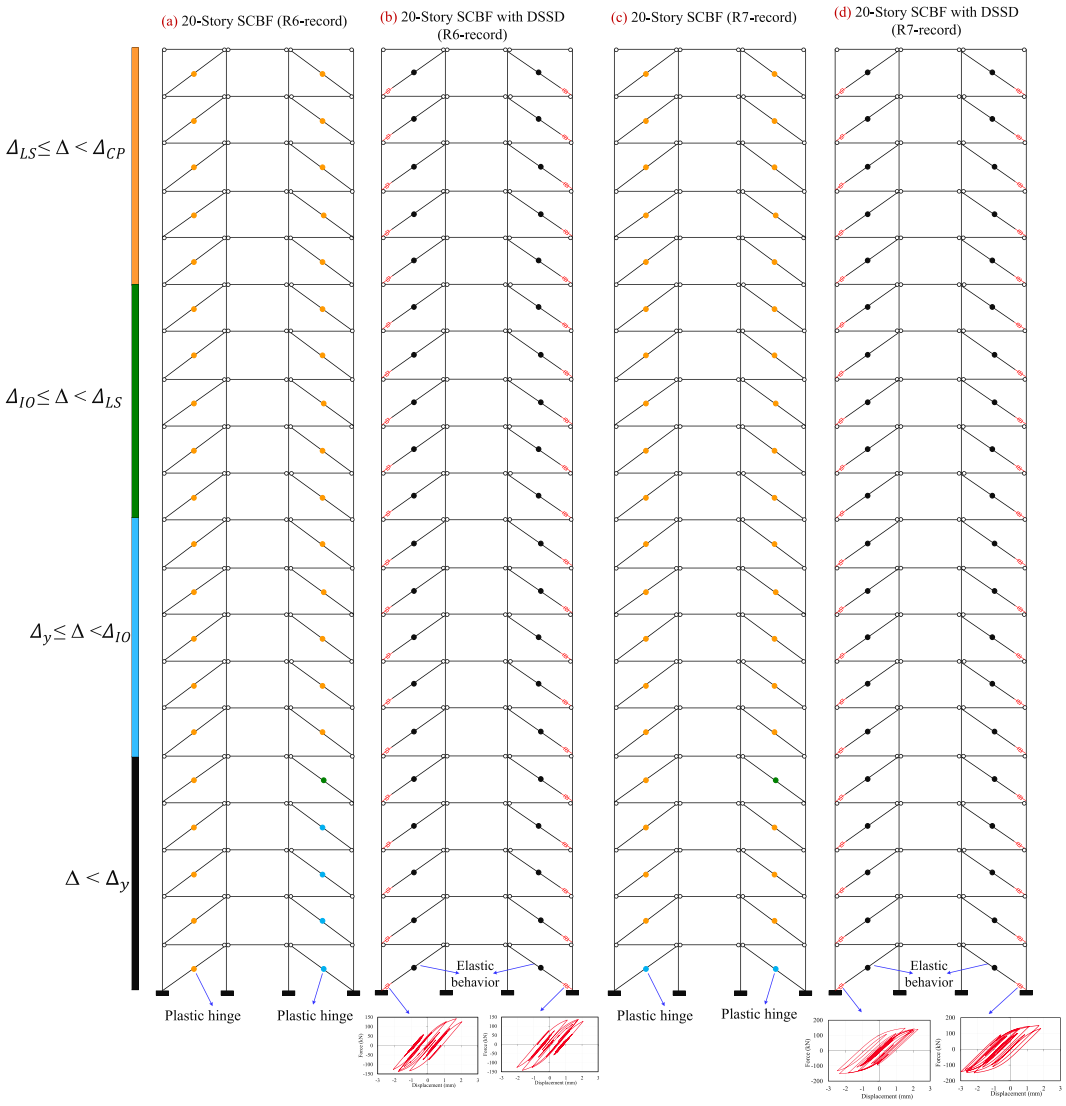

Fig. 38. Plastic hinging of 20-story SCBFs with and without DSSD: (a)–(b) record R6, and (c)–(d) record R7.

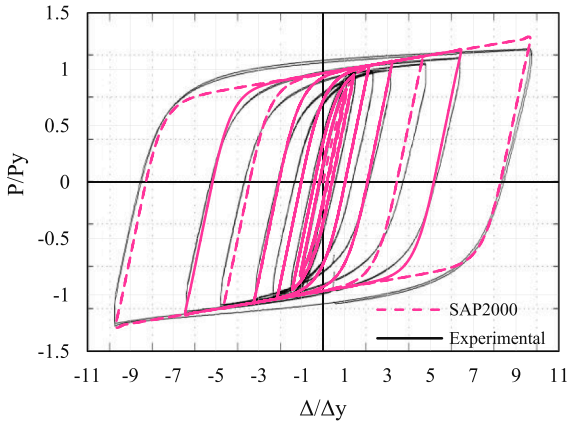

Fig. 39. SAP2000® vs experimental [70] hysteresis curves.

Table 6
Comparison of maximum base shear (kN).

ID	4-story Frame			8-story Frame		
	with BRB	with DSSD	Reduction (%)	with BRB	with DSSD	Reduction (%)
R1	250.6	187.6	25.1	531.1	288.1	45.8
R2	537.6	274.1	49.0	1047.0	408.4	61.0
R3	377.2	235.9	37.4	921.6	322.4	65.0
R4	379.2	239.1	36.9	727.6	362.5	50.2
R5	341.3	213.5	37.4	760.0	311.5	59.1
R6	491.0	274.8	44.1	825.5	337.0	59.2
R7	319.0	208.7	34.6	739.4	349.9	52.7
R8	262.0	190.0	27.5	456.2	203.0	55.5
R9	243.2	189.7	22.0	578.2	298.3	48.4
Average	**355.7**	**223.7**	**37.1**	**731.8**	**320.1**	**56.3**

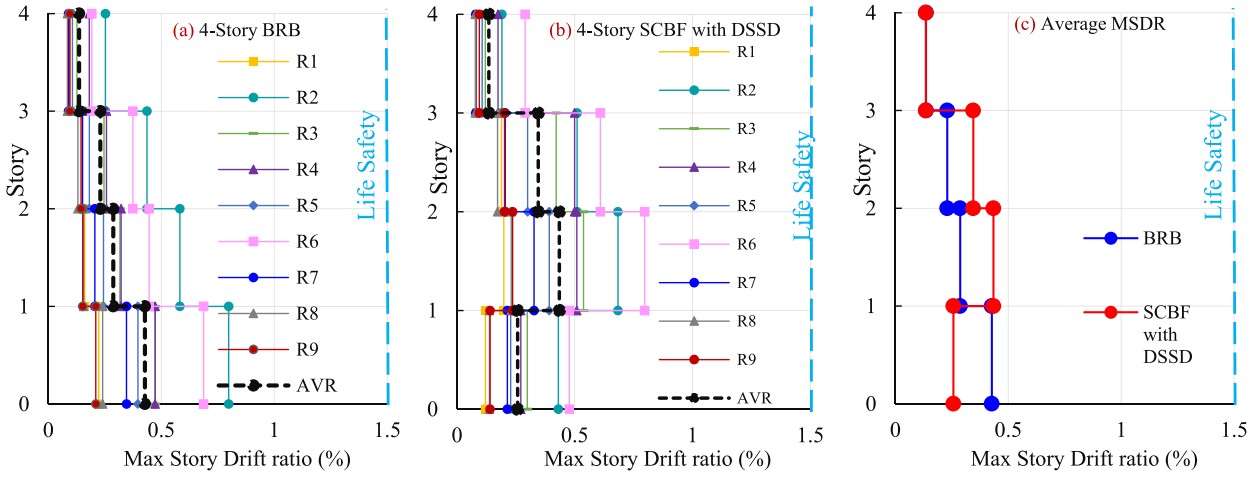

Fig. 40. MSDR of 4-story frames under seismic records: (a) BRBF, (b) SCBF with DSSD, (c) average MSDR.

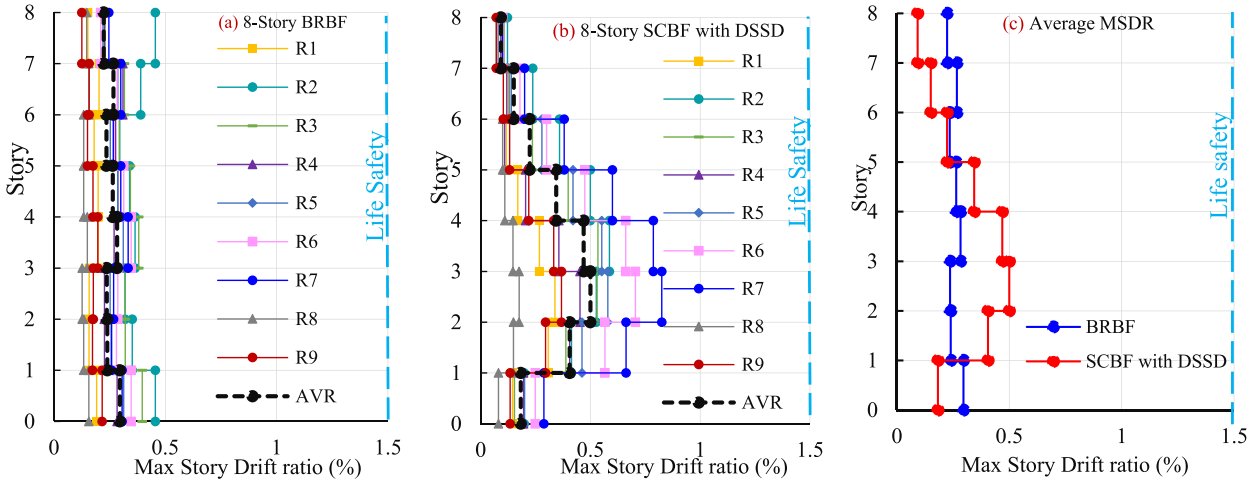

Fig. 41. MSDR of 8-story frames under seismic records: (a) BRBF, (b) SCBF with DSSD, (c) average MSDR.

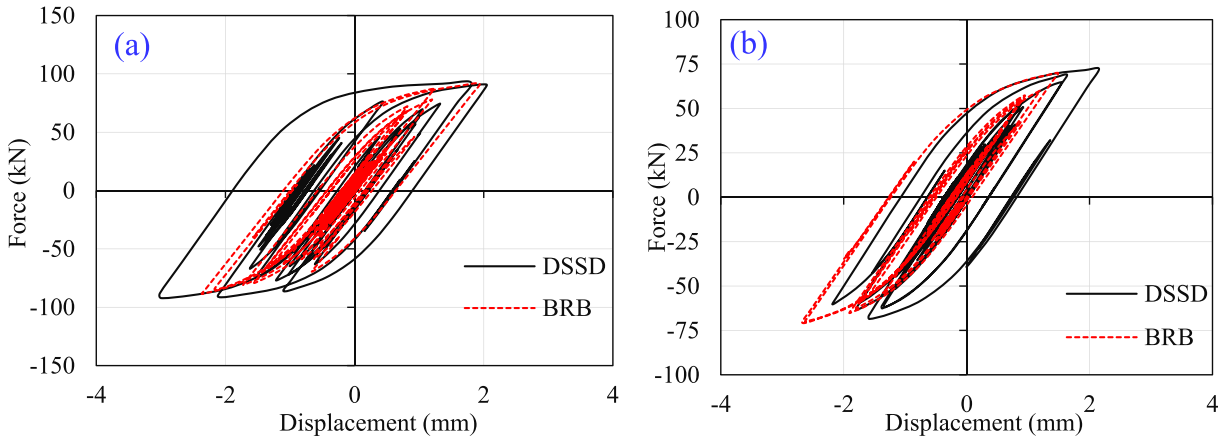

Fig. 42. Hysteresis curves comparison of BRB and DSSD subjected to record R1: (a) 6th-story, (b) 7th-story.

Plastic-Wen link element effectively captures BRB behavior.

Table 6 compares the maximum base shear of BRBFs and SCBFs with DSSD under the earthquake records. Although both systems had identical yield strength and stiffness, SCBFs with DSSD offered lower maximum base shear than BRBFs. This difference can be attributed to the higher post-yield stiffness of BRBs [71]. Specifically, the 4 and 8-story SCBFs with DSSD developed 37.1% and 56.3% lower average maximum base shear, respectively, compared to their counterpart BRBFs.

Figs. 40a–c and Figs. 41-c compare the MSDR of 4-story and 8-story frames subjected to the seismic records. In the 4-story frames (Fig. 40a–c), the BRBF developed lower MSDR in the middle stories (second and third stories), while it experienced higher MSDR in the first and top story, compared to SCBF with DSSD. The 8-story results (Figs. 41a–c) show a similar pattern, where BRBF had lower MSDR in the middle stories (second to fifth stories) but it developed higher MSDR in the first and upper three stories, compared to SCBF with DSSD. The lower MSDR in the middle stories of the BRBFs can be attributed to the higher post-yield stiffness of the BRB compared to the DSSD [71]. However, smaller displacements at the top stories can prevent BRBs from yielding efficiently, thus limiting their hysteretic response and energy dissipation capacity. Consequently, the BRBs cannot effectively control the seismic response of the frame, thereby producing higher MSDRs than the SCBF with DSSDs. Taking the R1 record as an example, Fig. 42 compares the hysteresis curves of the BRB and DSSD at stories 6 and 7. The fuller hysteresis loops of DSSDs confirm their superior energy dissipation at the upper stories, when compared to BRBs. Overall, compared to the BRBF, the SCBF with DSSD provides comparable performance in terms of MSDR and it also offers lower maximum base shear and easier replacement after a seismic event.

Based on the results presented in this article, it is concluded that the new DSSD is effective at improving the hysteretic response and energy dissipation capacity of braces, as well as at preventing the buckling of braces. Furthermore, the DSSD can enhance the structural response of SCBFs by reducing the maximum base shear and concentrating damage at the damper itself. It should be noted that whilst this article focused on assessing the behavior of the new DSSD via numerical analyses, further research is needed to evaluate different types of steel (such as low-yield point steel), the effect of the number of stiffeners, as well as the effect of different loading protocols, including large displacement cycles. Likewise, the explicit assessment of low-cycle fatigue and of fracture criteria of the DSSD requires experimental and numerical investigation to ensure its appropriate performance under seismic loads. It should also be noted that whilst the reference experiments adopted in the numerical calibration in Abaqus® reported negligible pinching effects, such effects can be important in slit dampers. As such, future research should examine potential pinching effects in the new DSSD. Moreover, different types of earthquake records, such as near-field records, also need to be investigated. Additionally, tests on actual full-scale DSSD are necessary to fully confirm the findings of this study.

9. Conclusions

Based on the results presented in this article, the following conclusions are drawn.

1. The numerical results indicate that the new DSSD dissipates energy through a stable hysteresis response without stiffness or strength degradation. Results from the parametric analysis confirm that increasing the thickness of the slit plates t (from 8 to 20 mm), slit plates length L (from 100 to 250 mm), and stiffener thickness b_s (from 6 to 12 mm) increased the maximum strength of the DSSD by up to 126.2%, 207.3%, and 64.2%, respectively. Likewise, increasing t, L, and b_s to such values also enhanced the energy dissipation capacity by 133%, 177%, and 56%, respectively. In contrast, increasing the damper height h reduced the strength (up to 71%) and energy dissipation capacity (up to 78%) of the DSSD. Changing the thickness of the stiffeners t_s had a minor effect on the DSSD's hysteresis response.
2. The numerical results indicate that the degradation factor of bare braces was $\lambda_i < 1$, thus suggesting buckling failure of the braces. On the other hand, braces with DSSD had $\lambda_i \geq 1$ in both tension and compression, which in turn increased energy dissipation by up

to 189% over conventional braces. Moreover, 99% of the energy was dissipated by the new DSSD, thus confirming that (as intended) the damper worked as a structural "fuse" and concentrated all damage.

3. The results from nonlinear time history analyses revealed that the use of DSSDs reduced the average maximum base shear of the 4, 8 and 20-story SCBFs by 57.8%, 54.3% and 47.8%, respectively. Moreover, the maximum story drift ratio (MSDR) of all SCBFs with DSSDs satisfied the Life Safety performance level (MSDR<1.5%) suggested in FEMA 356. However, further research considering different parameters and tests on actual DSSD are necessary to fully confirm the findings presented in this study.
4. The comparison between BRBFs and DSSDs demonstrated that SCBFs fitted with DSSD provided comparable seismic performance in terms of MSDR and offered up to 56.3% lower average maximum base shear for the case studies investigated here, along with easier damage assessment and replacement after a seismic event.

CRediT authorship contribution statement

Samaneh Jalal: Writing – original draft, Visualization, Software, Methodology, Investigation, Formal analysis. **Yashar Bakhshayesh:** Writing – original draft, Visualization, Supervision, Resources, Project administration, Methodology, Investigation, Funding acquisition, Formal analysis, Conceptualization. **Bahram Mirzaie Abar:** Writing – original draft, Validation, Supervision, Resources, Project administration, Investigation, Funding acquisition, Conceptualization. **Reyes Garcia:** Writing – review & editing, Writing – original draft, Visualization, Validation, Methodology, Data curation. **Iman Hajirasouliha:** Writing – review & editing, Visualization, Validation, Data curation.

Declaration of competing interest

The authors declare that they have no known competing financial interests or personal relationships that could have appeared to influence the work reported in this paper.

Appendix A

Summary of DSSD design calculation (specimen DSSDH190)

Description	Calculations (units: N, mm)
Step 1: Calculate (P_y) according to Eqs. (6)–(8).	$P_{y1} = min\left\{\frac{nF_y tb^2}{2h}, \frac{2nF_y tb}{3\sqrt{3}}\right\}$
	$= min\left\{\frac{8\times250\times8\times16.5^2}{2\times122}, \frac{2\times8\times250\times8\times16.5}{3\sqrt{3}}\right\} = min\{17852.5, 101613.6\} = 17852.5$
	$P_{y2} = min\left\{\frac{n'F_y t_s {b_s}^2}{2H}, \frac{2n'F_y t_s b_s}{3\sqrt{3}}\right\}$
	$= min\left\{\frac{8\times250\times20\times6^2}{2\times190}, \frac{2\times8\times250\times20\times6}{3\sqrt{3}}\right\} = min\{3789.5, 92376.04\} = 3789.5$
	$P_y = P_{y1} + P_{y2} = 17852.5 + 3789.5 = 21642$
Step 2: Calculate (P_{design}) according to Eq. 9.	$P_{design} = \Omega \times P_y = 1.98 \times 21642 = 42851$
Step 3: Check the middle plate capacity according to Eqs.10 to 12.	Assume the dimensions of middle plate: length: 150 mm, width: 100 mm, thickness: 10 mm
	$P_{design} \le \Phi P_n \rightarrow 42851 \le 0.9\times216839 \rightarrow 42851 \le 195155 \rightarrow thickness = 10$ mm ✓ OK
	$F_e = \frac{\pi^2 E}{\left(\frac{L_c}{r}\right)^2} = 733 \rightarrow \frac{F_y}{F_e} = \frac{250}{733} = 0.34 \le 2.25 \rightarrow P_n = \left(0.658^{\frac{F_y}{F_e}}\right)F_y A_g = \left(0.658^{0.34}\right)\times250\times100\times10 =$ 216839
Step 4: Check the boundary plates capacity according to Eq. 13.	Assume the dimensions of boundary plates: length: 150 mm, width: 100 mm, thickness: 25 mm
	$\frac{P_r}{P_c} = 0.07 < 0.2 \rightarrow$ Eq.13b$\rightarrow \frac{P_r}{2P_c} + \frac{M_r}{M_c} \le 1 \rightarrow \quad \frac{42851}{2\times610784} + \frac{4070845}{3906250} = 1.06$ ✓ OK
	$P_r = P_{design} = 42851 \quad M_r = M_{design} = P_{design} \times \frac{H}{2} = 42851 \times \frac{190}{2} = 4070845$
	$P_c = P_n\ (Eq.11) = 610784 \quad M_c = Z \times F_y = 3906250$

Data availability

No data was used for the research described in the article.

References

[1] Sac Joint Venture Guidelines Development Committee, et al., Recommended Seismic Evaluation and Upgrade Criteria for Existing Welded Steel moment-frame Buildings, vol. 351, Federal Emergency Management Agency, 2000.
[2] T.A. Horton, I. Hajirasouliha, B. Davison, Z. Ozdemir, More efficient design of reduced beam sections (RBS) for maximum seismic performance, J. Constr. Steel Res. 183 (2021) 106728.
[3] B.M. Abar, M.S. Ghobadi, Double shear bolted bracket moment connections, part 1: Four-bolt configuration design methodology, J. Constr. Steel Res. 174 (2020) 106280.
[4] B.M. Abar, Y. Bakhshayesh, R. Garcia, I. Hajirasouliha, A new energy-dissipating RBS connection with double-nut-bolts: seismic performance assessment and design methodology, Eng. Struct. 293 (2023) 116596.
[5] R.A. Jazany, I. Hajirasouliha, H. Farshchi, Influence of masonry infill on the seismic performance of concentrically braced frames, J. Constr. Steel Res. 88 (2013) 150–163.
[6] A.D. Sen, M.A. Swatosh, R. Ballard, D. Sloat, M.M. Johnson, C.W. Roeder, D.E. Lehman, J.W. Berman, Development and evaluation of seismic retrofit alternatives for older concentrically braced frames, J. Struct. Eng. 143 (5) (2017) 04016232.
[7] C.W. Roeder, A.D. Sen, C. Terpstra, S.M. Ibarra, R. Liu, D.E. Lehman, J.W. Berman, Effect of beam yielding on chevron braced frames, J. Constr. Steel Res. 159 (2019) 428–441.
[8] M. Khademi, M. Tehranizadeh, A. Shirkhani, I. Hajirasouliha, Earthquake-induced loss assessment of steel dual concentrically braced structures subjected to near-field ground motions, Structures 51 (2023, May) 1123–1139.
[9] A. Kachooee, M.A. Kafi, A suggested method for improving post buckling behavior of concentric braces based on experimental and numerical studies, Structures 14 (2018, June) 333–347.
[10] Y. Bakhshayesh, M. Shayanfar, A. Ghamari, Improving the performance of concentrically braced frame utilizing an innovative shear damper, J. Constr. Steel Res. 182 (2021) 106672.
[11] A. Ramezantitkanloo, M.A. Kafi, A. Kachooee, Numerical study of concentrically braced frames with the replaceable reduced section under cyclic loading, Asian Journal of Civil Engineering 25 (1) (2024) 461–476.
[12] S.E. Dursun, C. Topkaya, Development of H-shaped hysteretic dampers for steel concentrically braced frames, Soil Dynam. Earthq. Eng. 166 (2023) 107758.
[13] S. Ebrahimi, S.R. Mirghaderi, A new friction–slip brace damper to improve seismic performance of braced frames, J. Constr. Steel Res. 207 (2023) 107945.
[14] M. Wang, K. Dong, M. Liu, Damage control mechanism and seismic performance of a steel moment connection with replaceable low-yield-point steel double T-stub fuses, Thin-Walled Struct. 157 (2020) 107143.
[15] Q. Xie, State of the art of buckling-restrained braces in Asia, J. Constr. Steel Res. 61 (6) (2005) 727–748.
[16] R. Sabelli, S. Mahin, C. Chang, Seismic demands on steel braced frame buildings with buckling-restrained braces, Eng. Struct. 25 (5) (2003) 655–666.
[17] V. Mohsenian, N. Gharaei-Moghaddam, I. Hajirasouliha, Reliability analysis and multi-level response modification factors for buckling restrained braced frames, J. Constr. Steel Res. 171 (2020) 106137.
[18] B.L. Zhu, Y.L. Guo, P. Zhou, M.A. Bradford, Y.L. Pi, Numerical and experimental studies of corrugated-web-connected buckling-restrained braces, Eng. Struct. 134 (2017) 107–124.
[19] F. Wang, Q.X. Shi, P. Wang, Seismic behaviour of reinforced concrete frame structures with all steel assembled Q195 low yield buckling restrained braces, Structures 30 (2021, April) 756–773.
[20] A. Benavent-Climent, A brace-type seismic damper based on yielding the walls of hollow structural sections, Eng. Struct. 32 (4) (2010) 1113–1122.
[21] F. Shao, T. Gu, L.J. Jia, H. Ge, M. Taguchi, Experimental study on damage detectable brace-type shear fuses, Eng. Struct. 225 (2020) 111260.
[22] R. Ullah, M. Vafaei, S.C. Alih, A. Waheed, Investigating the seismic response of chevron braced frame equipped with a replaceable sandwiched fused damper, J. Build. Eng. 86 (2024) 108928.
[23] S.M.S. Alehashem, A. Keyhani, H. Pourmohammad, Behavior and performance of structures equipped with ADAS & TADAS dampers (a comparison with conventional structures), Proc. of the 14th World Conference on Earthquake Engineering 12 (2008, October) 17.
[24] M. Khazaei, Investigation on dynamics nonlinear analysis of steel frames with steel dampers, Procedia Eng. 54 (2013) 401–412.
[25] M. Khoshkalam, M.H. Mortezagholi, S.M. Zahrai, Proposed modification for ADAS damper to eliminate axial force and improve seismic performance, J. Earthq. Eng. 26 (10) (2022) 5130–5152.
[26] M. Mahmoudi, M.G. Abdi, Evaluating response modification factors of TADAS frames, J. Constr. Steel Res. 71 (2012) 162–170.
[27] M. TahamouliRoudsari, M.B. Eslamimanesh, A.R. Entezari, O. Noori, M. Torkaman, Experimental assessment of retrofitting RC moment resisting frames with ADAS and TADAS yielding dampers, Structures 14 (2018) 75–87.
[28] R.W. Chan, F. Albermani, Experimental study of steel slit damper for passive energy dissipation, Eng. Struct. 30 (4) (2008) 1058–1066.
[29] S.H. Oh, Y.J. Kim, H.S. Ryu, Seismic performance of steel structures with slit dampers, Eng. Struct. 31 (9) (2009) 1997–2008.
[30] B. Hwang, T. Kim, Y. Kim, J. Kim, A comparative study on hysteretic characteristics of austenitic stainless steel and carbon steel slit dampers under cyclic loading. Journal of Building *Engineering* 45 (2022) v103553.
[31] K. Nik-Hoosh, M.A. Kafi, Experimental investigation into effect of strip or slit geometric pattern on structural and seismic behavior of steel slit yield damper and determining optimal pattern under cyclic loading, Journal of Structural and Construction Engineering 8 (5) (2021) 5–23.
[32] M.A. Shayanfar, M.A. Barkhordari, A.R. Rezaeian, Experimental study of cyclic behavior of composite vertical shear link in eccentrically braced frames, Steel Compos. Struct. 12 (1) (2012) 13–29.
[33] S.M. Zahrai, A. Moslehi Tabar, Analytical study on cyclic behavior of chevron braced frames with shear panel system considering post-yield deformation, Can. J. Civ. Eng. 40 (7) (2013) 633–643.
[34] S.M. Zahrai, Cyclic testing of chevron braced steel frames with IPE shear panels, Steel Compos. Struct. 19 (5) (2015) 1167–1184.
[35] L.Y. Xu, X. Nie, J.S. Fan, Cyclic behaviour of low-yield-point steel shear panel dampers, Eng. Struct. 126 (2016) 391–404.
[36] J. Wang, J. Men, Q. Zhang, D. Fan, S. Qi, C.H. Huang, Cyclic behavior of a shape-optimized dumbbell-type combined slit damper with phased yielding characteristic, J. Build. Eng. 88 (2024) 109216.
[37] S. Demir, M. Husem, Saw type seismic energy dissipaters: development and cyclic loading test, J. Constr. Steel Res. 150 (2018) 264–276.
[38] R. Ullah, M. Vafaei, S.C. Alih, A. Waheed, A replaceable sandwiched metallic fuse damper for seismic protection of braced frames, Eng. Struct. 298 (2024) 117072.
[39] F. Taiyari, F.M. Mazzolani, S. Bagheri, A proposal for energy dissipative braces with U-shaped steel strips, J. Constr. Steel Res. 154 (2019) 110–122.
[40] S.S. Askariani, S. Garivani, Introducing and numerical study of a new brace-type slit damper, Structures 27 (2020, October) 702–717.
[41] S.B. Beheshti Aval, S. Ghayoumi, I. Hajirasouliha, Numerical Study of cyclic performance and design of a novel fan bracing system, J. Earthq. Eng. 26 (12) (2022) 6494–6523.
[42] M.G. Gray, C. Christopoulos, J.A. Packer, Cast steel yielding brace system for concentrically braced frames: concept development and experimental validations, J. Struct. Eng. 140 (4) (2014) 04013095.
[43] M. Almohammad-Albakkar, F. Behnamfar, Numerical investigation of grooved gusset plate damper for using in cross-braced frames, J. Constr. Steel Res. 196 (2022) 107434.
[44] G. Pachideh, M. Kafi, M. Gholhaki, Evaluation of cyclic performance of a novel bracing system equipped with a circular energy dissipater, Structures 28 (2020, December) 467–481.
[45] F. Behnamfar, A. Ahmadi, A.G. Anaraki, V. Mazrouei, Performance evaluation of concentrically braced frames equipped with pure bending yielding damper, Structures 58 (2023, December) 105650.
[46] F. Kazemi, N. Asgarkhani, N. Lasowicz, R. Jankowski, Development and experimental validation of a novel double-stage yield steel slit damper-buckling restrained brace, Eng. Struct. 315 (2024) 118427.

[47] V. Rodriguez-Moreno, H. Guerrero, J.A. Escobar, A. Teran-Gilmore, Cyclic behavior of a slit damper proposed for precast concrete beam-column connections, Eng. Struct. 294 (2023) 116745.
[48] A.M. Rousta, M.G. Azandariani, M.A.S. Ardakani, S. Shoja, Cyclic behavior of an energy dissipation system with the vertical steel panel flexural-yielding dampers, Structures 45 (2022, November) 629–644.
[49] ANSI/AISC 360-16, Specification for Structural Steel Buildings, American Institute of Steel Construction (AISC), Chicago, Illinois, USA, 2016.
[50] Abaqus, Analysis User's Manual 6.14, Dassault Systemes Simulia Corp., Providence, RI, 2011.
[51] K.H. Nip, L. Gardner, A.Y. Elghazouli, Cyclic testing and numerical modelling of carbon steel and stainless steel tubular bracing members, Eng. Struct. 32 (2) (2010) 424–441.
[52] F. Xu, W.H. Pan, T.M. Chan, T. Sheehan, L. Gardner, Fracture prediction for square hollow section braces under extremely low cycle fatigue, Thin-Walled Struct. 171 (2022) 108716.
[53] B.M. Abar, M.S. Ghobadi, New generation of bolted bracket connections: safe load-carrying capacity and structural damage assessment, Eng. Struct. 252 (2022) 113662.
[54] B.M. Abar, M. D'Aniello, R. Landolfo, An extension of EC8-concepts to AISC-like design criteria for ductile stainless steel end-plate moment connections, Eng. Struct. 332 (2025) 120035.
[55] FEMA 461, Federal Emergency Management Agency, Interim Protocols for Determining Seismic Performance Characteristics of Structural and Nonstructural Components, 2007. Washington, DC, USA.
[56] W. Wang, Q. Luo, S. Xu, B. Wang, Z. Sun, Application research of corrugated mild metal shear damper based on damage control and energy-dissipation improvement, J. Build. Eng. 47 (2022) 103840.
[57] W.Y. Liu, G.Q. Li, J. Jiang, Experimental study on reinforced concrete frames with two-side connected buckling-restrained steel plate shear walls, Adv. Struct. Eng. 21 (3) (2018) 460–473.
[58] H. Azizi, J. Ahmadi, F. Kazemi, Enhancing seismic resilience in steel frames with synchronized double-stage yield buckling-restrained braces, Soil Dynam. Earthq. Eng. 198 (2025) 109587.
[59] RHUDRC, in: 2800-Standard for Design of Structures Against Earthquakes, fourth ed., Road, Housing and Urban Development Research Center, Teheran, Iran, 2014.
[60] CSI, SAP2000 v.20 integrated finite element analysis and design of structures, in: Computers and Structures, Inc., 2020. Berkeley, USA.
[61] American Society of Civil Engineers, in: Seismic Evaluation and Retrofit of Existing Buildings, Report ASCE/SEI 41-13, Reston, VA, 2014.
[62] N.D.K.R. Chukka, M. Krishnamurthy, Seismic performance assessment of structure with hybrid passive energy dissipation device, Structures 27 (2020, October) 1246–1259.
[63] A. Naeem, J. Kim, Seismic performance evaluation of a multi-slit damper, Eng. Struct. 189 (2019) 332–346.
[64] FEMA P695, Quantification of Building Seismic Performance Factors. Report No. P695, Federal Emergency Management Agency, Washington, DC, USA, 2009.
[65] V. Mohsenian, I. Hajirasouliha, R. Filizadeh, Seismic reliability analysis of steel moment-resisting frames retrofitted by vertical link elements using combined series–parallel system approach, Bull. Earthq. Eng. 19 (2) (2021) 831–862.
[66] V. Mohsenian, R. Filizadeh, I. Hajirasouliha, R. Garcia, Seismic performance assessment of eccentrically braced steel frames with energy-absorbing links under sequential earthquakes, J. Build. Eng. 33 (2021) 101576.
[67] B. Besharatian, H.T. Riahi, R. Garcia, I. Hajirasouliha, A practical optimisation method for friction tuned mass dampers in multi-storey buildings subjected to earthquake excitations, Soil Dynam. Earthq. Eng. 184 (2024) 108857.
[68] B. Besharatian, H.T. Riahi, R. Garcia, I. Hajirasouliha, Particle swarm optimization of friction tuned mass dampers subjected to ground motion records, Soil Dynam. Earthq. Eng. 172 (2023) 107995.
[69] FEMA, Commentary for the Seismic Rehabilitation of Buildings (FEMA 356), Federal Emergency Management Agency, Washington, DC, USA, 2000.
[70] C. Black, I.D. Aiken, N. Makris, Component testing, stability analysis, and characterization of buckling-restrained unbonded braces (TM). Pacific Earthquake Engineering Research Center, 2002.
[71] C. Qiu, X. Du, Seismic performance of multistory CBFs with novel recentering energy dissipative braces, J. Constr. Steel Res. 168 (2020) 105864.
[72] B. Qu, C. Dai, J. Qiu, H. Hou, C. Qiu, Testing of seismic dampers with replaceable U-shaped steel plates, Eng. Struct. 179 (2019) 625–639.
[73] E. Nyabongo, X. Li, Development of energy-early-dissipated braces based on web buckling of low-yield I-section steel, J. Constr. Steel Res. 217 (2024) 108672.